The role of the lipid droplet binding protein Plin4 in the development of non-alcoholic steatohepatitis

Absence of Plin4 alleviates hepatic expression of inflammatory and fibrotic genes in mice fed an MCD diet

Selma Wibe Fjellberg

Master in Clinical Nutrition
60 credits

Department of Nutrition
Faculty of Medicine
University of Oslo

May 2021

The role of the lipid droplet binding protein Plin4 in the development of non-alcoholic steatohepatitis

Absence of Plin4 alleviates hepatic expression of inflammatory and fibrotic genes in mice fed an MCD diet

Selma Wibe Fjellberg

Master in Clinical Nutrition
60 credits

Department of Nutrition
Faculty of Medicine
University of Oslo

May 2021

Supervisors:

Associate Professor Knut Tomas Dalen

Postdoctoral Researcher Marit Hjorth

2021

The role of the lipid droplet binding protein Plin4 in the development of non-alcoholic steatohepatitis

Absence of Plin4 alleviates hepatic expression of inflammatory and fibrotic genes in mice fed an MCD diet

Selma Wibe Fjellberg

https://www.duo.uio.no/

Trykk: Reprosentralen, Universitetet i Oslo

Abstract

Introduction: The prevalence of obesity and insulin resistance is increasing worldwide and is closely associated with development of non-alcoholic fatty liver disease (NAFLD). Hepatic accumulation of TAG sequestered in cytosolic lipid droplets (LDs) is an important step in the development of NAFLD. This has linked LD metabolism and its associated proteins, such as the Perilipin (Plin) family, to the disease progression of NAFLD. Previous research has revealed potential roles of Plin2, Plin3, and Plin5 in NAFLD, but the role of Plin4 has not been explored.

Materials and methods: The role of Plin4 in the development of non-alcoholic steatohepatitis (NASH) was investigated by feeding *Plin4*$^{+/+}$ and *Plin4*$^{-/-}$ male and female mice a methionine and choline sufficient (MCS) or methionine and choline deficient (MCD) diet for two weeks. Body- and organ-weights, hepatic TAG accumulation, plasma ALT levels, and selected metabolic plasma markers were measured. RT-qPCR was used to measure hepatic mRNA expression levels of genes related to inflammation and fibrosis, LD-surface stabilization, and hepatic lipid metabolism. Hepatic expression of Plin2, Plin3, Plin5, and α-SMA proteins was measured by immunoblotting.

Results: The primary finding of this master project was that *Plin4*$^{-/-}$ male mice receiving an MCD diet for two weeks had attenuated induction of several genes related to inflammation, fibrosis, and macrophages compared to *Plin4*$^{+/+}$ male mice receiving the same diet. Additionally, we showed that MCD feeding induced hepatic mRNA and protein expression of Plin5 in *Plin4*$^{+/+}$ mice, whereas Plin5 induction was attenuated in *Plin4*$^{-/-}$ mice fed the same diet.

Conclusion: This study is the first to demonstrate a potential role of Plin4 in NAFLD. With the use of a common dietary model for development of NASH in mice, we showed that the absence of Plin4 seems to slow the progression towards NASH by alleviating the expression of inflammatory and fibrotic gene markers normally induced by an MCD diet.

Acknowledgements

This master thesis was conducted at the Department of Nutrition at the Faculty of Medicine, University of Oslo, from August 2020 to May 2021. First, I wish to show my gratitude to my supervisor, Associate Professor Knut Tomas Dalen, for your expert guidance throughout the year. The time you have spent discussing both my master project and the research field with me has increased my knowledge and interest. You have been a great support during the writing process and your feedback has really brought my master thesis to a higher level.

I wish to give a special thank you to my supervisor, Postdoctoral Researcher Marit Hjorth. During the master year, you have spent a lot of time teaching me all I need to know about laboratory work. With all your knowledge, you have been of importance to me during the writing process, and you have always helped me in challenging times. Your instructive feedback surely made my master thesis better. I will thank both my supervisors for always being available for answering questions I might have had, which has helped me stay on the right track during the entire year.

I will also thank Atanaska, Ingunn, Shaista, and Frode for the warm welcome and for including me in the research environment. Thank you to all my good study friends. Without you, these past five years would never have been the same. Thank you for all the laughter, good times, and support. I also want to thank my mom, dad, sister, and brother for supporting and calming me down during stressful periods.

Lastly, I will give a warm and special thank you to my boyfriend, Claes-Henning. You have been my biggest support and motivator during this year. You have countless times helped me calm down. I look forward to our coming time together.

Oslo, May 2021

Selma Wibe Fjellberg

List of abbreviations

Abhd5: Abhydrolase Domain Containing 5

Acaca: Acetyl-CoA Carboxylase Alpha

ACC: Acyl-CoA carboxylase

Acetyl-CoA: Acetyl coenzyme A

Acox1: Acyl-CoA Oxidase 1

Adgre: Adhesion G Protein-Coupled Receptor E1

ALT: Alanine aminotransferase

ANOVA: Analysis of variance

ATGL: Adipose triglyceride lipase

ATP: Adenosine triphosphate

BCA: Bicinchoninic acid

BMI: Body mass index

BSA: Bovine serum albumin

cDNA: Complementary deoxyribonucleic acids

CE: Cholesteryl ester

Chrebp: Carbohydrate-responsive element-binding protein

Cide: Cell death-inducing DFF45-like effector

Col1a1: Collagen Type I Alpha 1 Chain

Cpt1a: Carnitine Palmitoyltransferase 1A

CPT: Carnitine Palmitoyltransferase

CVDs: Cardiovascular diseases

Dmpk: Myotonic dystrophy protein kinase

DNase: Deoxyribonuclease

dNTP: Deoxynucleotide triphosphate

dsDNA: Double stranded deoxyribonucleic acid

ECM: Extracellular matrix

ER: Endoplasmic reticulum

ES cell: Embryonic stem cell

FA: Fatty acid

Fasn: Fatty Acid Synthase

FFA: free fatty acid

G0s2: G0/G1 Switch 2

HF diet: High-fat diet

HKG: Housekeeping gene

HSC: Hepatic stellate cells

HSL: Hormone-sensitive lipase

HUNT: The Trøndelag-Health Study

Il1b: Interleukin 1 Beta

Il6: Interleukin 6

IR: Insulin resistance

IVC: Individually ventilated cages

LD: Lipid droplet

Lipe: Lipase E, Hormone Sensitive Type

LT: Liver transplant

Lyz: Lysozyme

Marco: Macrophage Receptor With Collagenous Structure

MCD: Methionine and choline deficient diet

MCS: Methionine and choline sufficient diet

MQ H_2O: Milli-Q water

NAFL: Non-alcoholic fatty liver

NAFLD: Non-alcoholic fatty liver disease

NASH: Non-alcoholic steatohepatitis

PC: Phosphatidylcholine

Plin: Perilipin

Pnpla2: Patatin Like Phospholipase Domain Containing 2

PPARs: Peroxisome proliferator-activated receptors

Ppib: Peptidyl-Prolyl Cis-Trans Isomerase B

RIPA: Radio-immunoprecipitation assay buffer

RNA: Ribonucleic acid

RNase: Ribonuclease

ROS: Reactive oxygen specie

Rpm: Round per minute

RT: Reverse transcriptase enzyme

RT-q-PCR: Reverse transcriptase quantitative polymerase chain reaction

S2 cell: Schneider 2 cells

SCAT: Subcutaneous adipose tissue

SDS-PAGE: Sodium dodecyl sulphate–polyacrylamide gel electrophoresis

Srebf1: Sterol Regulatory Element Binding Transcription Factor 1

SREBP1c: Sterol regulatory element-binding protein 1c

ssDNA: Single stranded deoxyribonucleic acid

TAG: Triglyceride

TF: Transcription factor

Tgfb1: Transforming growth factor beta1

Tnf: Tumor Necrosis Factor

USA: United States of America

VAT: Visceral fat

VLDL: Very low density lipoprotein

WC: Waist circumference

WHO: World Health Organization

α-SMA: Alpha Smooth Muscle Actin

List of tables

List of figures

List of appendices

Table of Contents

1 Introduction

1.1 Overweight and obesity

The prevalence of overweight and obesity has risen dramatically over the past three decades and is now widely regarded as a global pandemic (1). The rise is found in both developed and developing countries and poses a serious challenge to global health, because of its associated comorbidities such as type 2 diabetes, hypertension, cardiovascular diseases (CVDs), and non-alcoholic fatty liver disease (NAFLD) (1-4). There are many factors behind the increased prevalence, such as economic growth, industrialization, urbanization, increased sedentary lifestyles, and unhealthy eating patterns characterized by increased consumption of processed and energy-dense foods of low nutritional value (3). However, the key mechanism behind the population's weight gain is an energy intake exceeding the body's energy consumption (2, 5).

Most epidemiologic studies use body mass index (BMI) to classify individuals as overweight or obese (3, 6). BMI is calculated by dividing body weight in kilograms by the height in meter squared (kg/m^2) (6). The World Health Organization (WHO) defines overweight as a BMI equal to or greater than 25, and obesity as a BMI equal to or greater than 30 (7). BMI is an effective classification tool but does not take body composition into consideration (8), thus being an indirect measure of obesity (6). As the comorbidities related to obesity are highly dependent on body fat distribution rather than the total body fat mass (9, 10), waist circumference (WC) is another measurement tool commonly used for classifying obesity. WC is a good indicator for abdominal fat, which mostly consists of visceral fat (11).

In 1980, the global proportion of overweight among adults (>18 years) was found to be 29% for men and 30% for women (1). In 2013, these numbers had increased to 37% and 38%, for men and women, respectively (1). In 2016, WHO estimated the prevalence of obesity in the adult population (>18 years) to be 13% (7). This was nearly a tripling since 1975 (7). Data from The Trøndelag-Health Study (HUNT) have revealed increasing trends in the prevalence of overweight and obesity in the Norwegian population between HUNT1 (performed in 1984-1986) and HUNT3 (performed in 2006-2008) (12). During this time frame, overweight prevalence increased from 42% to 52% in men, and 30% to 38% in women, while obesity prevalence increased from 8% to 21% in men and from 13% to 23% in women (12).

The subcutaneous adipose tissue (SCAT) is the main buffer for storing excess energy in the form of triglycerides (TAG), and thus protects other tissues from depositing fat (13). However, the storing capacity of the SCAT can be exceeded, which results in an accumulation of fat in other areas of the body not optimized for lipid storage, such as the insides of the abdominal cavity, known as visceral fat (VAT) (13). VAT differs physiologically and metabolically from SCAT (13). It is more metabolically active, with a greater rate of lipolysis, higher levels of inflammatory cells, and more insulin resistant (13). Accumulation of VAT is associated with NAFLD development. The venous blood flow from VAT drains directly to the liver via the portal vein, and thus feeds the liver with free fatty acids (FFA) as well as different adipokines, which increase the risk of developing liver steatosis and inflammation (13-15) .

1.2 The liver

1.2.1 Anatomy

The human liver is formed as a triangular pyramid (16), weighing approximately 1500 grams, and is placed in the upper right abdominal quadrant right under the diaphragm (17, 18). The organ is systematically build up by hepatocytes, endothelial cells, Kupffer cells and, stellate cells (19). It consists of many lobuli. Each hepatic lobule is formed as a hexagon, with a central hepatic vein and a portal triad in each corner, consisting of branches from the bile duct, portal vein, and hepatic artery (19). This organization creates a zonal heterogeneity, where the metabolic processes conducted by the hepatocytes are adapted to the composition of their surrounding microenvironment (19).

1.2.2 The role of liver in metabolism

Because of its location and many important functions, the liver is critical in maintaining the body's energy homeostasis. The liver is the first organ to access and manage the majority of ingested nutrients because of its blood drainage from the gastrointestinal tract through the portal vein (20). These nutrients can further be metabolized and stored in the liver or sent to peripheral tissues and cells (20). Fatty acids (FA) with more than 12-14 carbons are an exception to this (21). They are packed in chylomicrons in the enterocytes and transported to peripheral tissues via the lymph and blood circulation before the chylomicron remnant enters the liver (21).

The liver plays a key role in buffering blood glucose levels, with its capability to both store (glycogenesis) and synthesize (gluconeogenesis) glucose (22). The activity of the different metabolic pathways are tightly regulated by neuronal and hormonal signals, where insulin and glucagon play important roles (20). In the fasted state, the liver buffers blood glucose levels by glycogen breakdown and *de novo* synthesis of glucose through gluconeogenesis (22). The precursors used in gluconeogenesis are mainly glycerol, lactate, and glucogenic amino acids (23). During periods of fasting, the glycogen storage will gradually deplete, and the release of FFAs from adipose tissue becomes an important energy source for the organism (23). In the liver, the FAs are oxidized and used as an energy source and for the production of ketone bodies (20). The ketone bodies, circulating FFA, and the *de novo* synthesized glucose become the major energy sources for extrahepatic tissues, such as the brain, heart, and skeletal muscle in periods of prolonged fasting (23). In contrast to nutrient deprivation, the liver can also handle periods of excess nutrient supply, such as in the fed state, when insulin levels are increased. The liver uses excess glucose to refill its glycogen storage (glycogenesis) and for FA synthesis through *de novo* lipogenesis (20).

1.2.3 Lipid metabolism in the liver

De novo lipogenesis

The starting point for *de novo* lipogenesis is acetyl-CoA, mainly derived from excess glucose, but also from other substrates, such as fructose (24, 25). The major enzymes catalysing the transformation of acetyl-CoA into FAs are acyl-CoA carboxylase (ACC), and fatty acid synthase (FASN) (14). ACC carboxylates acetyl-CoA into malonyl-CoA (20), which further is converted into FAs (mainly palmitate) by FASN (25). The synthesized FAs may be elongated to form long-chain fatty acids and desaturated (20). Finally, TAG is formed by the esterification of three FAs with glycerol-3-phosphate (25). The TAG may be stored in hepatic lipid droplets (LD) or secreted as very low density lipoprotein (VLDL) particles for delivery of FAs to peripheral tissues, such as adipose tissue (25, 26).

A diet rich in carbohydrates increase the rate of hepatic *de novo* lipogenesis (27). Both lipogenic enzymes and transcription factors (TF) are activated upon glucose and insulin signalling in the hepatocytes (28). Activated lipogenic TFs, such as sterol regulatory element-binding protein 1c (SREBP1c) and carbohydrate-responsive element-binding protein (ChREBP), induce the transcription of genes involved in *de novo* lipogenesis and TAG

synthesis (14, 28). Dysregulation and increased activity of hepatic *de novo* lipogenesis is associated with the development of liver steatosis (24, 28).

Oxidation of lipids

During periods of nutrient deprivation, such as fasting, elevated levels of catecholamines enhance lipolysis in adipocytes (29-31). TAG stored in LDs is hydrolysed, resulting in secretion of FFAs and glycerol into the bloodstream (30). The hydrolysis of TAG is mediated by the action of lipolytic enzymes such as adipose triglyceride lipase (ATGL) and hormone-sensitive lipase (HSL) (30), encoded by the genes *Pnpla2* and *Lipe*, respectively. Peripheral tissues and the liver utilize the FFA for energy production through β-oxidation and subsequent production of adenosine triphosphate (ATP) (31, 32).

FAs taken up by cells must be activated by the conversion to fatty acyl-CoA before they can be utilized (32). β-oxidation of FAs occurs in the mitochondrial matrix, with the exception of very long-chain fatty acids and branched-chain fatty acids that are oxidized in the peroxisome (33). Short- and medium-chain fatty acids can directly enter the mitochondria matrix, but long-chain fatty acids need to be transported by the carnitine shuttle (33). This transport system depends on the activity of the two enzymes carnitine palmitoyltransferase (CPT) I and II and a translocase (33, 34). β-oxidation of FAs produces acetyl-CoA, which can enter the citric acid cycle and partake in cellular respiration to produce ATP (33). In addition, the liver has a unique ability to convert the acetyl-CoA into ketone bodies (33).

Peroxisome proliferator-activated receptors (PPARs) are a nuclear receptor family of transcription factors important in the regulation of lipid homeostasis (35, 36). The family consists of PPARα, PPARδ, and PPARγ (36). Upon binding of ligands (mainly various FAs), they form heterodimers with the retinoid X receptor and regulate gene expression of numerous genes involved in lipid metabolism (35). PPARα and PPARδ are primarily expressed in metabolically active tissues and stimulate FA catabolism, while PPARγ is mainly expressed in adipose tissue, where it is important in adipocyte differentiation and the storage of fat (35, 37). PPARγ is also prominently expressed in macrophages (35, 37).

PPARα is highly expressed in the liver (38), where it plays an important role in regulating FA handling, especially in circumstances where the FA delivery is increased, for example during starvation (35). Upon activation, PPARα controls the expression of several genes involved in FA utilization (35), such as *Acox1* and *Cpt1*, two central enzymes in β-oxidation (37, 39). In addition to its role in FA metabolism, PPARα has been found to have anti-inflammatory effects, especially in the vascular wall and the liver (37, 40).

1.3 Lipid droplets

More attention has been given to the biology of LDs in the last decades, as it has become clear that disturbances in LD metabolism and accumulation of LDs are tightly connected with several diseases such as obesity, CVDs, NAFLD, and lipodystrophies (41).

LDs are dynamic cellular organelles specialized in storage of neutral lipids and have pivotal roles in lipid and energy homeostasis (41-43). The organelle is composed of a hydrophobic core consisting of neutral lipids, mainly TAG and cholesteryl ester (CE), surrounded by a phospholipid monolayer (41-45). Several types of proteins with various functions, primarily structural and regulatory, are found to associate with the LD membrane (41, 46). In addition to their role as energy reservoirs, the neutral lipids are used as building blocks for biological membranes and various signalling molecules (42, 45-47). The ability to sequester excess FAs and sterols as neutral lipids in LDs is also a protective mechanism to hinder cellular lipotoxicity and oxidative stress that can cause insulin resistance, inflammation, and cell death, hallmarks that are closely associated with the pathophysiology of NAFLD (41, 42, 45, 48).

The formation of LDs occurs in the endoplasmic reticulum (ER) where the enzymes needed for neutral lipid synthesis reside (41, 44). As neutral lipids are synthesized, an oil lens starts to form within the leaflets of the ER bilayer (41). The oil lens will eventually bud from the ER membrane and become a nascent LD that further matures within the cytosol (41). Nearly all cells have the ability to form LDs (43, 44, 47, 49), but the lipid droplet size and neutral lipid composition vary between cells and sometimes even within the same cell (41, 44, 50).

The synthesized LDs disperse into the aqueous cytosol (42, 44, 47), where their stability is controlled by molecules at the water-oil interface (42, 44). These serve as surfactants, with variable abilities to lower the lipid droplet surface tension (47, 51). The most important ones are the phospholipids that comprise the LD membrane, with phosphatidylcholine (PC) being the most abundant one (47). PC is found to have a crucial role in stabilizing the LD emulsion and hinder LD coalescence (42, 44, 47, 52).

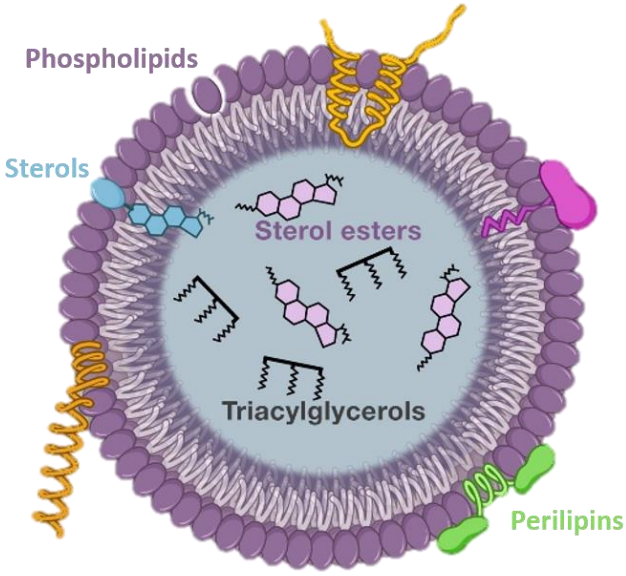

Figure 1.1: Structure of a lipid droplet. Lipid droplets consist of a core of natural lipids, mainly triacylglycerol and cholesteryl ester, surrounded by a monolayer of phospholipids. Several types of proteins are associated with the membrane, such as proteins from the Perilipin family. The figure is modified from Farese and Walther (53) and reused with permission.

1.3.1 Perilipins

Perilipins (Plins) are an evolutionarily related family of LD coating proteins (54). They are found in a wide variety of animal species highlighting their crucial role in regulating LD metabolism (55). Mammalian genomes contain five *Plin* genes encoding the Plin proteins *Plin1* to *Plin5*, sequentially named after their time of discovery (45). The protein family shares a great similarity in their N-terminus and central region, which are strongly conserved across species (45). All Plins comprises two protein motifs; an N-terminal PAT-domain of ~100 amino acids present in all family members, although less conserved in Plin4, followed by a centrally located 11-mer repeated region of variable length, with the longest repeat found in Plin4 (45, 54-56). The 11-mer repeat region is believed to fold into amphipathic alpha helixes that are important for the binding of Plins to LDs (57).

The LD membrane is always decorated with at least one member of the Plin family (41, 45). While Plin1 and Plin2 are degraded unless they are associated with the LD membrane, the other Plin family members may reside freely or be associated with other components of the cytosol (45, 50, 55, 58). The expression pattern of the Plins differs between tissues, which indicates that the different members have specialized functions matching the tissue's role in lipid metabolism (44-46). Plin1 is mainly expressed in adipocytes and

steroidogenic cells (54), where it serves as an important regulator of lipolysis (58, 59). Plin2 and Plin3 are abundantly expressed and associated with LDs of most cells (45, 54, 58), with the LDs of hepatocytes being predominated by Plin2 (50). Plin5 is highly expressed in tissues with high levels of mitochondrial β-oxidation, such as heart, skeletal muscle, brown adipose tissue, and the liver (43, 60, 61).

1.3.2 Perilipin 4

Plin4 is the least studied Plin protein, and little is known about its physiological function (56). As already mentioned, the protein is distinct from the other Plin family members, with an expanded 11-mer repeated region of about 900 amino acids and a less conserved PAT-domain (45, 55, 56). The expression of Plin4 is most abundant in white adipose tissue, with lower expression in heart and skeletal muscle (43). Activation of PPARγ stimulates expression of Plin4 in adipocytes (62). When cultured adipocytes are exposed to high levels of fatty acids, Plin4 is found to coat nascent small LDs close to the cell membrane, which suggests that the protein is involved in the early stages of LD formation (63). In other cultured cells, Plin4 is found to associate with LDs containing CE but be nearly absent from LDs containing TAG (64). *Plin4*$^{-/-}$ mice have reduced cardiac TAG levels, but it is unclear if this is indirectly caused by reduced mRNA and protein expression of Plin5 in heart, white adipose tissue, and the liver in absence of Plin4 (65).

1.4 Non-Alcoholic Fatty liver disease

NAFLD has become the leading cause of liver disease in western countries because of its close association with obesity and insulin resistance (26). NAFLD includes a spectrum of diseases ranging from milder forms to more severe conditions, which all have developed in the absence of alcohol abuse (normally defined as an alcohol intake <30 grams and <20 grams per day for men and women, respectively) (26). The disease spectrum includes simple steatosis, often referred to as non-alcoholic fatty liver (NAFL) (characterized by TAG infiltration in more than 5% of hepatocytes) and non-alcoholic steatohepatitis (NASH) (characterized by the presence of additional inflammation and hepatocyte injury), which further may progress into liver fibrosis and cirrhosis which again increase the risk of developing hepatocellular carcinoma (26, 66, 67). Since NAFLD in many cases appears asymptomatic (68), and with the lack of an accurate, sensitive, and non-invasive marker for NAFLD, it has been hard to estimate its precise prevalence (69). The gold standard for

diagnosing NAFLD is liver histology (26, 48), but this method is also the most invasive (67). Liver function tests, especially blood levels of alanine aminotransferase (ALT), have frequently been used as markers for chronic liver disease. However, such tests may fluctuate and appear normal in patients with NAFLD (69-71). Abdominal ultrasonography is now the most used and recommended diagnostic method for NAFLD (26, 48).

The prevalence of NAFLD varies between countries, continents, age, and sex. It rises with age and is found to be higher in men than in women (26, 48, 72, 73). A meta-analysis from 2016 found the global prevalence of NAFLD diagnosed by imaging to be 25.24%, with the highest prevalence in the Middle East (31.8%) and South America (30.5%), and the lowest in Africa (13.5%) (73). The prevalence in Europe and North America was found to be 24% (73). In a study conducted in the connection with the Trøndelag Health study 3 (HUNT3) the prevalence of NAFLD was found to be 36% in a Norwegian population of 15 781 participants from 20 years and older (74).

Over the next 20 years, NAFLD is predicted to become the primary cause of liver-related morbidity and mortality, and already within a decade become the major indicator for liver transplant (LT) (66, 75). In the Nordic countries, the percent of patients awaiting LT due to NAFLD has increased from 2% in 1994-1995, to 6.2% in 2011-2015 (76). In comparison, the frequency of conducted NAFLD related LTs in the United States of America (USA) has increased from 1.2% in 2001 to 9.7% in 2009 (77), and is today the second leading cause of LT in the USA (78). As of now, the most effective therapy for NAFLD is lifestyle changes, such as increased physical activity, weight loss, and dietary changes (79, 80). With the increasing prevalence of NAFLD, intense research is ongoing to develop safe and effective therapeutic targets (81, 82).

1.4.1 Pathogenesis of NAFLD

The pathogenesis of NAFLD is complex and multifactorial and occurs normally over years at a slow rate (14, 83). Several factors such as obesity, insulin resistance (IR), microbiome changes, and predisposing genetic variations are involved, but the pathogenesis is still not fully understood (14, 84). Hepatic TAG accumulation, caused by an imbalance between FA utilization and storage, is thought to be the first step in the development of NAFLD (14, 24). The key sources for the accumulated hepatic TAG are FAs derived from adipocyte lipolysis, dietary fat intake, and hepatic *de novo* lipogenesis (14). Insulin resistance is an important driver in the pathogenesis (85). With IR, insulin fails to inhibit lipolysis in

adipocytes, resulting in an increased release of FFAs into the circulation, which mostly are taken up by the liver (14, 85). This FFA flux has been measured to constitute for 60% of the accumulated liver TAG in NAFLD patients (86). The hyperinsulinemia that develops as a consequence of IR stimulates the activity of *de novo* lipogenesis in the liver (25, 87).

Progression from NAFL to NASH

Progression towards NASH among patients with NAFL varies and depends on the time perspective, but is found to occur in 44% of NAFL patients over a 6-year period (88). The liver's response to the excessive influx of FAs, by converting them into TAG followed by sequestration into LDs, is a protective mechanism against cellular lipotoxicity (48). Therefore, TAG accumulation in hepatocytes is likely not the trigger for hepatocyte injury, which is seen in NASH livers (48). Rather, the development of NASH is a result of hepatic lipotoxicity, which occurs when the flux of FFAs within the hepatocytes exceeds the cell's handling capacity (14, 48). This results in the formation of toxic lipid metabolites, such as ceramides and diacylglycerols (48).

Lipotoxicity causes the onset of cellular-stress, -injury, and -death through mechanisms such as production of reactive oxygen species (ROS) and induction of ER-stress (14, 87, 89). These processes induce inflammatory responses that further aggravates the rate of cellular injury and death (89). The release of stress signals from the injured cells and elevations in inflammatory signals will activate resident immune cells such as Kupffer cells and dendritic cells, and also attract bone marrow-derived cells, such as macrophages (90, 91). This will initiate wound healing and repair responses, which eventually can lead to fibrosis and cirrhosis development (90). Fibrosis is characterized by an increased deposition of extracellular matrix (ECM) proteins, such as collagen type I and III (92). The increased deposition of ECM proteins may disturb normal physiological processes such as nutrient transport through the liver parenchyma (92). Activated hepatic stellate cells (HSC) are major contributors in the production of ECM components in fibrotic livers (14).

HSC are mesenchymal cells, which in normal conditions are found in a quiescent state (14, 91, 92). With LDs rich in retinylpalmitate, they constitute the body’s main storage site for vitamin A (14, 91, 92). Upon stimulation by transforming growth factor beta1 (TGF- β1), secreted by cell types such as Kupffer cells, recruited macrophages, and hepatocytes HSCs transdifferentiate into myofibroblasts (14, 48, 91, 92). In this process they lose their intracellular LDs storage of retinylpalmitate, gain contractile properties, significantly increase

their expression of α-SMA (92), become the major producer of ECM components, secrete cytokines (91), and proliferate (14).

1.4.2 Methionine and choline deficient diet as an animal model to study NAFLD

To study the disease spectrum of NAFLD, different dietary and genetic animal models are used (93), which all differ in their ability to mimic the natural development of NAFLD in humans (83). The methionine and choline deficient (MCD) diet is the most used dietary model to induce NAFLD/NASH in mice (94). Dietary lack of these essential nutrients rapidly induces hepatic steatosis, due to an increased uptake and decreased secretion and utilization of lipids (83). Methionine and choline deficiency reduces the availability of the two important precursors for phosphatidylcholine biosynthesis (95). Since PC biosynthesis is required for the assembly and normal secretion of VLDL particles, MCD feeding will impair this process (83, 96, 97). The diet also causes liver damage with increased liver inflammation and oxidative stress, as well as hepatic fibrosis over a prolonged feeding period (83).

Although the MCD diet induces hepatic lipid accumulation and hepatocyte injury, the disease manifestation is limited to the liver. The mice are not obese nor insulin resistant, which normally is associated with the natural pathogenesis of NAFLD (83). They rather develop cachexia and lose significant amounts of adipose tissue and bodyweight (83, 98). The use of the MCD diet as a dietary model to study the pathogenesis of NAFLD should therefore be restricted to the liver.

1.4.3 NAFLD and Perilipins

Hepatic accumulation of TAG sequestered in cytosolic LDs is an important step in NAFLD development. This has linked LD metabolism and its associated proteins to the disease progression (99). The expression of *Plin1*, *Plin2*, *Plin3*, *and Plin5* are found to be induced in steatotic livers of both humans and mice (100-103), suggesting that these are important constituents of LDs in NAFLD. Previous research has revealed potential roles of Plin2, Plin3, and Plin5 in NAFLD (102-105). Currently, no reported studies have investigated whether Plin4 is implicated in the pathogenesis of NAFLD. The main objective of this master project was therefore to cover this knowledge gap and search for potential roles of Plin4 in the development of NASH.

1.5 Aims and hypothesis

The overall goal of this master project was to investigate if Plin4 plays a role in the development of NASH. The project is based on a conducted diet intervention where *Plin4*$^{+/+}$ and *Plin4*$^{-/-}$ mice had been fed a methionine and choline deficient (MCD) diet to induce development of NASH, or a control methionine and choline sufficient (MCS) diet. Biological material and phenotype data collected from *Plin4*$^{+/+}$ and *Plin4*$^{-/-}$ mice fed the MCS or the MCD diet were analysed in this master study.

<u>The specific aims were as follows:</u>
Plin4$^{+/+}$ and *Plin4*$^{-/-}$ mice were fed an MCS or an MCD diet to analyse the following:

- Body- and organ-weights
- Plasma and liver TAG
- Metabolic plasma markers and markers for liver damage
- If the absence of Plin4 resulted in compensatory expression of related lipid droplet binding proteins in the liver
- Hepatic gene and protein markers for development of NASH
- Expression levels of genes central for hepatic lipid metabolism
- Sex differences in the development of NASH in response to MCD feeding

2 Material and Methods

2.1 Material

Material used for data collection and molecular analyses

Table 2.1. **Equipment.** Equipment used to perform molecular analyses and data collection.

Equipment	Producer
ABI Prism 96-Well Optical Reaction Plate	Applied Biosystems (Foster City, US)
Bioruptor Plus® sonication device	Diagenode (Liège, Belgium)
Bioruptor® Water Cooler	Diagenode (Liège, Belgium)
Centrifuge, Biofuge fresco	TermoFisher Scientific (Waltham, MA, US)
Centrifuge, Mini Spi, Eppendorf	Eppendorf AG (Hamburg, Germany)
Centrifuge, Mini Spi, PCR Strips	TermoFisher Scientific (Waltham, MA, US)
CFX96 Real-Time System Thermal Cycler	Bio-Rad Laboratories (Hercules, CA, US)
ChemiDoc™ Touch Imaging System	Bio-Rad Laboratories (Hercules, CA, US)
Criterion™ Cell system	Bio-Rad Laboratories (Hercules, CA, US)
Criterion™ TGX™ Gel, 26 Well Comb, 15 µl, 4-20%	Bio-Rad Laboratories (Hercules, CA, US)
Eppendorf Research Plus Pipettes	Eppendorf AG (Hamburg, Germany)
Eppendorf tubes	Sarstedt (Germany)
Falcon tubes	Falcon, Corning Incorporation (Durham, US)
Filter paper	Bio-Rad Laboratories (Hercules, CA, US)
Glass beads (1 mm)	Glass beads, Assistant, (Germany)
Gloves	Kimtech, Kimberly-Clark Professional
Mastercycler Ep Gradient S	Eppendorf AG (Hamburg, Germany)
Microseal, B'Adhesive Seals for PCR Plates	Bio-Rad Laboratories (Hercules, CA, US)
Microtest Plate 96 Well F	Sarstedt (Germany)
Micro tubes	Sarstedt (Germany)
Multi-channel pipette	Eppendorf Research (Germany)
Nano Drop ND-1000 Spectrophotometer	TermoFisher Scientific (Waltham, MA, US)
PCR strips with attached caps	TermoFisher Scientific (Waltham, MA, US)
Pipette tips, Biosphere (5mL, 10mL)	Falcon, Corning Incorporation (Durham, US)
Pipette tips (0.5-10 µl, 0.1-20 µl, 2-100 µl, 2-200 µl,1250 µl)	Eppendorf Research Plus (Hamburg, Germany)
Pipetboy acu 2	Integra Bioscience (Hudson, US)
PowerPac™ Basic	Bio-Rad Laboratories (Hercules, CA, US)
PreLys24 Homogenizer	Bertin Instruments (France)
Synergy H1™ Hybrid Multi-Mode Reader	BioTek (Winooski, VT, US)
Trans-Blot® Turbo™ Transfer System	Bio-Rad Laboratories (Hercules, CA, US)

Table 2.2: Kits. Kits used to perform molecular analyses and data collection.

Kit	Producer
Cholesterol Reagent Set	Pointe Scientific Inc. (Canton, MI, USA)
Glucose (Oxidase) Reagent Set	Pointe Scientific Inc. (Canton, MI, USA)
High-Capacity cDNA Reverse Transcription Kit	Applied Biosystems (Warrington, UK)
NucleoSpin RNA kit	Macherey-Nagel (Düren, Germany)
Pierce™ BCA Protein Assay Kit	TermoFisher Scientific (Waltham, MA, US)
Pointe ALT (SGPT) Reagent Set	Pointe Scientific Inc. (Canton, MI, USA)
Triglyceride (GPO) Reagent Set	Pointe Scientific Inc. (Canton, MI, USA)
Trans-Blot® Turbo™ RTA Transfer Kit, Nitrocellulose (Midi-size)	Bio-Rad Laboratories (Hercules, CA, US)

Table 2.3: Chemicals and reagents. Chemicals and reagents used to perform molecular analyses and data collection.

Chemicals and reagents	Producer
α-Smooth Muscle Actin, Rabbit	Cell Signalling Technology
Beta-mercaptoethanol	Sigma-Aldrich (St. Louis, MO, US)
Bovine serum albumin (BSA)	Sigma-Aldrich (St. Louis, MO, US)
Bromophenol blue sodium salt	Sigma-Aldrich (St. Louis, MO, US)
Chow diet	Research Diets INC (US)
DL-Dithiothreitol	Sigma-Aldrich (St. Louis, MO, US)
Donkey Anti-Guinea Pig IgG (H+L)	Jackson ImmunoResearch (PA, US)
Dry ice	Praxair (Guildford, UK)
EDTA	Sigma-Aldrich (St. Louis, MO, US)
Ethanol (EtOH) 96%	Sigma-Aldrich (St. Louis, MO, US)
GAPDH, Rabbit	Santa Cruz Biotechnology
Glycerol (>99.0%)	Sigma-Aldrich (St. Louis, MO, US)
Glycine	Sigma-Aldrich (St. Louis, MO, US)
Goat Anti-Rabbit IgG	Jackson ImmunoResearch (PA, US)
Hydrochloric acid	Sigma-Aldrich (St. Louis, MO, US)
Methanol (> 99.9%)	Sigma-Aldrich (St. Louis, MO, US)
Methionine and choline sufficient diet	Research Diets INC (US)
Methionine and choline deficient diet	Research Diets INC
Milli-Q water (MQ H_2O)	Millipore (Massachusetts, US)
Nonidet™ P 40, 100%	Sigma-Aldrich (St. Louis, MO, US)
PCR-grade water	Sigma-Aldrich (St. Louis, MO, US)
Perilipin 2 (C-terminus), Guinea pig	Progen (Heidelberg, Germany)
Perilipin 3 (N-Terminus), Guinea pig	Progen (Heidelberg, Germany)
Perilipin 5 (C-Terminus), Guinea pig	Progen (Heidelberg, Germany)
Phenol:Chloroform:Isoamylalcohol (25:24:1)	Invitrogen (Life technologies, Paisley, UK)
Phosphate-buffered saline (PBS)	Sigma-Aldrich (St. Louis, MO, US)
Phosphatase inhibitor	Sigma-Aldrich (St. Louis, MO, US)
Precision Plus Protein™ Standards (All Blue)	Bio-Rad Laboratories (Hercules, CA, US)
Precision Plus Protein™ Standards (Dual Color)	Bio-Rad Laboratories (Hercules, CA, US)
Primers (see appendix 2)	Sigma-Aldrich (St. Louis, MO, US)
Protease inhibitor	Boehringer Mannheim
RA1 Lysis Buffer	Macherey-Nagel (Düren, Germany)
Sample buffer, Laemmli (4x concentrate)	Sigma-Aldrich (St. Louis, MO, US)
Sodium chloride, NaCl ((Physiological concentration of 150 mM)	Sigma-Aldrich (St. Louis, MO, US)
Sodium dodecyl sulfate (SDS)	Sigma-Aldrich (St. Louis, MO, US)
Sodium deoxycholate	Sigma-Aldrich (St. Louis, MO, US)
Sodium chloride (NaCl)	Sigma-Aldrich (St. Louis, MO, US)
SsoAdvanced Universal SYBR Green Supermix	Bio-Rad Laboratories (Hercules, CA, US)
SuperSignal® West Pico Chemiluminiscent Substrate	TermoFisher Scientific (Waltham, MA, US)
Tris base	Sigma-Aldrich (St. Louis, MO, US)
Tris-HCl	Sigma-Aldrich (St. Louis, MO, US)
Tween® 20	Sigma-Aldrich (St. Louis, MO, US)

Table 2.4: Computer software. Computer software used to perform analysis, collection, and processing of data.

Program	Producer
EndNote X9.2	Thomson Reuters
CFX Manager 3.1 Software	Bio-Rad Laboratories (Hercules, CA, US)
Gen5 Microplate Reader and Imager Software v3.02	BioTek (Winooski, VT, US)
GraphPad Prism 8 Software	GraphPad Software Inc. (San Diego, CA, US)
Image J 1.50i	National Institutes of Health, USA
Image Lab™ Software	Bio-Rad Laboratories (Hercules, CA, US)
Microsoft Office 2016	Microsoft®
ND-1000 Software	Saveen & Werner AB, Sweden

2.2 Methods

2.2.1 Animal model and ethical considerations

The Lipid Droplet Research group has generated *Plin4* knock out mice (*Plin4*$^{-/-}$), with absence of Plin4, to characterize their phenotype. Several *in vivo* studies where *Plin4*$^{+/+}$ and *Plin4*$^{-/-}$ mice were fed different diets have been conducted to investigate how the absence of Plin4 influences storage, mobilization, and oxidation of lipids stored in LDs. The experimental use of animals was approved by Mattilsynet (FOTS portal) (FOTS protocol id #10901). Mice were housed and cared for in accordance with the ethical guidelines in Directive 2010/63/EU of the European Parliament and the ARRIVE guidelines.

2.2.2 Dietary model

In this master project, *Plin4*$^{+/+}$ and *Plin4*$^{-/-}$ mice were fed a methionine and choline deficient (MCD) diet to induce development of NASH, or a control methionine and choline sufficient (MCS) diet. The mice were backcrossed into the c57bl/6N strain for more than ten generations to create a congenic strain. Animals were housed in individually ventilated cages (IVC) in an animal facility that maintained a stable temperature at 22°C with 55% relative humidity and a 12 hours light/dark cycle (7 AM to 7 PM). The study included 20 *Plin4*$^{+/+}$ and 14 *Plin4*$^{-/-}$ male mice, and 18 *Plin4*$^{+/+}$ and 20 *Plin4*$^{-/-}$ female mice. The mice were fed chow until 12 weeks of age (containing 58E% carbohydrate, 18E% fat, and 24E% protein (Envigo, Indiana, USA)), then fed the MCS diet for one week before they were given the MCS or MCD diet for 2 additional weeks (Figure 2.1). The diets were custom made from Research diets, Inc. USA (MCD diet product #A02082002B, MCS diet product #A02082003B) (See table 2.5 for diet composition). The mice were permitted *ad libitum* consumption of food and

water. On the last intervention day, the mice were euthanized by cervical dislocation between 8 AM and 10 AM. Bodyweight was measured and blood samples collected before they got dissected for tissue collection. While dissecting, organ weights of heart, liver, kidney, epididymal-/periovarian-, and inguinal-fat depots were measured. The tissues were snap frozen in liquid nitrogen and kept at -80°C. All collections of biological materials were done before the initiation of this master project.

Table 2.5: Nutrient composition of the intervention diets. Nutrient composition presented in grams per 100 grams and energy percent (E%). Abbreviations: Carb: Carbohydrate; Met: Methionine; MCD: methionine and choline deficient diet; MCS: Methionine and choline sufficient diet.

	Diet composition, g/100g (E%)						
	Protein	**Fat**	**Carb**	**Sucrose**	**Met**	**Choline**	**Kcal/g**
MCD diet	17 (16.1)	9.9 (21.2)	65.9 (62.7)	45 (42.9)	0	0	4.2
MCS diet	17.5 (16.7)	9.9 (21.2)	50.7 (62.4)	44.7 (42.6)	0.3	0.2	4.2

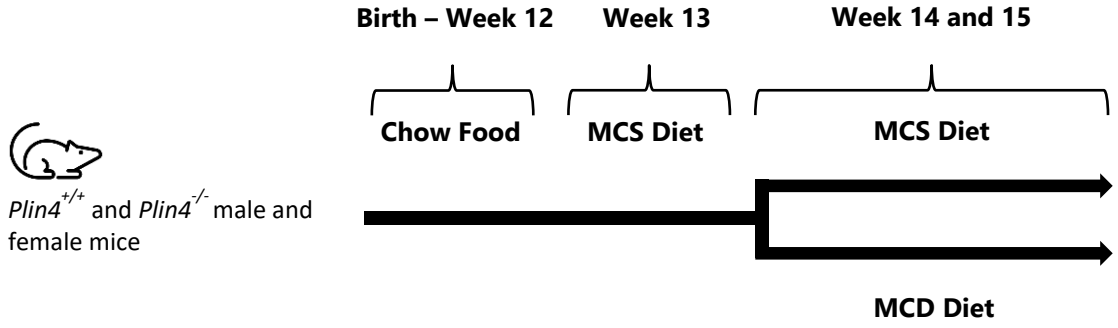

Figure 2.1: Timeline of the study. 20 *Plin4*$^{+/+}$ and 14 *Plin4*$^{-/-}$ male mice, and 18 *Plin4*$^{+/+}$ and 20 *Plin4*$^{-/-}$ female mice were included in the study. Mice were fed chow until 12 weeks of age, then given methionine and choline sufficient diet (MCS) for one week before mice were given MCS or methionine and choline deficient diet (MCD) for two additional weeks.

2.2.3 Quantitative reverse transcription polymerase chain reaction

The methionine and choline deficient diet is an often used model to study the pathophysiology of NAFLD/NASH in mice. Gene expression analyses restricted to liver tissue were used to evaluate liver damage, expression levels of genes related to LD binding, and hepatic lipid metabolism. Gene expression levels were quantified with reverse transcriptase quantitative polymerase chain reaction (RT-q-PCR). This method quantifies the amount of complementary deoxyribonucleic acid (cDNA), which have been generated by

reverse transcription of ribonucleic acid (RNA) catalysed by a reverse transcriptase enzyme (RT).

Tissue homogenization and isolation of total RNA

Total RNA from liver tissue was isolated using a NucleoSpin RNA kit (Macherey-Nagel, Düren, Germany). The instructions accompanying the kit were followed, except for two modifications that included a Phenol-Chloroform extraction step and the addition of a high salt solution. Approximately 5 mg of liver tissue stored in RNAlater was transferred to microtubes with 10-15 glass beads and lysis buffer (RA1 buffer, Machery-Nagel, Düren, Germany) containing 1% β-mercaptoethanol. The samples were homogenized in a PreLys 24 homogenizer (Bertin instruments) for 2x30s at 5000 rpm. The samples were added 350 µl Phenol:Chloroform:Isoamyl Alcohol (25:24:1), shaken for 20 seconds and incubated at room temperature for two minutes before they were centrifuged at 9,000 rpm for five minutes. This separated the samples into three phases: an organic-, inter-, and aqueous phase. The highly polar nucleic acids remained in the aqueous phase, while other molecules such as proteins, lipids, and cellular debris dissolved into the organic phase and the interphase. The aqueous phase was carefully pipetted into new tubes (the yield was approximately 350 µl). A high salt precipitation was conducted to remove polysaccharide contamination in the samples, which will increase the RNA yield and purity when isolated from tissues with high glycogen content. The sample volume of ~350 µl was added 95 µl high salt solution (recipe in Appendix 1) and 260 µl 96% EtOH, both followed by vortexing. Finally, the total sample volume of approximately 700 µl was transferred to the column for further purification steps as described in the NucleoSpin RNA kit manual (Macherey-Nagel, Düren, Germany).

Determination of RNA concentration and purity

The concentration and purity of the isolated RNA was measured following the protocol written by Desjardins, P., & Conklin, D (106) using the NanoDrop ND-1000 spectrophotometer (Thermo Scientific, Waltham, MA). The absorbance levels at 260 nm were used to estimate the RNA concentration, while the 260/280 and 260/230 ratios were used to determine the RNA purity. Samples with a 260/280 ratio of ~2 and a 260/230 ratio of 2-2.2 were accepted as pure. Lower ratio levels indicated the presence of contaminants that absorb near or at 280 and 230 nm, such as proteins, phenols, guanidine, or carbohydrates.

cDNA synthesis

All samples were diluted with RNase free H_2O to achieve a common RNA concentration of 86 ng/µl. Total RNA was reverse transcribed into first strand cDNA using High Capacity cDNA Reverse Transcriptase Kit (Applied Biosystems) and its corresponding protocol. The components of the reverse transcriptase master mix were mixed (Table 2.6), including two negative control samples; One to confirm the absence of template contamination in the solutions of the master mix ("no-template" 5 µl RNAse free H_2O and 5 µl master mix) and one without the RT enzyme to control for DNA contamination in the RNA samples ("no-RT" 5 µl RNA collected from three random RNA samples and 4.5 µl master mix without the RT-enzyme). 5 µl of each RNA sample/H_2O were combined with 5 µl master mix to gain a total reaction volume of 10 µl. All samples, including controls, were placed in the Thermocycler (Mastercycler Ep Gradient S, Eppendorf AG (Hamburg, Germany)) with the following settings; Annealing: 10 minutes at 25°C (the primers bind to RNA); Reverse transcription: 120 minutes at 37°C (RNA is used as a template for the RT enzyme which incorporates complementary dNTPs to make cDNA); Enzyme inactivation: 5 minutes at 85°C (the heat inactivates the RT enzyme).

Table 2.6: Reverse transcriptase master mix recipe. Abbreviations: RNase: Ribonuclease; RT: reverse transcriptase; dNTP: deoxynucleotide triphosphate

Reagents	**Volume per sample (µl)**
RNase free H_2O	2.1
10X RT buffer	1
10X random primers	1
dNTPs	0.4
MultiScribe RT enzyme	0.5
Total volume	**5**

Real time quantitative PCR

10 µl of each cDNA sample was diluted in 90 µl RNAse free H_2O to achieve an expected cDNA concentration of 4.3 ng/µl. This dilution simplified pipetting and increased the accuracy of the RT-q-PCR results since a larger volume of the cDNA reaction was added to the qPCR reaction. A master mix (Table 2.7) containing a gene specific primer pair (Appendix 2) and SYBR Green (Sso Advances, Biorad) was made for each gene measured. 2.5 µL of the cDNA samples and the two negative controls made during cDNA synthesis were pipetted into a 96-well PCR plate and then added 7.5 µl master mix. The plate was

covered with a microseal film (Bio-Rad Laboratories (Hercules, CA, US)), the samples mixed, the plate spun down for 1 minute, then inserted in a CFX96 Real-Time System Thermal Cycler (Bio-Rad Laboratories (Hercules, CA, US)). The CFX Manager 3.1 Software (Bio-Rad Laboratories (Hercules, CA, US)) was used for cycling condition setup and Ct-value generation. The first initial denaturation step lasted for 3 minutes at 95°C, followed by 40 repetitive cycles of denaturation and annealing with the following cycling conditions: Denaturation: 10 seconds at 95°C (double stranded (ds) DNA separates into single stranded (ss) DNA); Annealing and extension: 20 seconds at 60°C (Primers bind to its target sequence and DNA-polymerase extend the primers by incorporating complementary dNTPs). The amount of amplicons generated was measured at the end of each cycle by the fluorescence light emitted by SYBR green intercalating with dsDNA. Generated Ct values were exported to Microsoft Excel and relative mRNA expression was calculated using the comparative ΔΔCt model with *Ppib* as reference gene (107).

Table 2.7: Components of the master mix for RT-qPCR. Template specific primer pairs (3´- and 5´- primers) were used to investigate relative mRNA expression of defined target genes (Appendix 2). SYBR Green was used to fluorescently label dsDNA amplified in the RT-qPCR reaction. Abbreviations: dsDNA: double stranded deoxyribonucleic acid; RT-qPCR: Quantitative reverse transcription polymerase chain reaction.

Components	Volume per sample (µl)
RNA-se free H_2O	5
SYBR Green mix	2.3
3'primer	0.1
5'primer	0.1
Total volume	7.5

2.2.4 Immunoblotting

Preparation of liver lysates

Frozen liver tissue samples of ~70 mg were transferred to 2 ml screw cap tubes with ~15 glass beads on dry ice. 100 µl RIPA lysis buffer (Appendix 3) was added per 10 mg liver tissue and the samples were homogenized for 2x30 sec at 6000 rpm in a PreLys24 homogenizer (Bertin Instruments). The liver lysates were sonicated with the maximum energy settings for 3x30 seconds in a Bioruptor® Plus sonication device (Diagenode).

Measurement of protein concentration

The protein concentration of each liver lysate sample was measured with a BCA Protein Assay (ThermoFisher Scientific, MA, US). An aliquot of each liver lysate was diluted 50 times with MQ H_2O. 25 µl of each dilute was pipetted into a 96 well plate together with eight standards with decreasing bovine serum albumin (BSA) (Sigma-Aldrich, MO, US) concentrations (2000 to 0 µg/µl). 200 µl BCA solution was added to each well, followed by mixing and incubating at 37°C for 30 minutes. Absorbance levels were measured at 562 nm in the Synergy H1™ Hybrid Multi-Mode Reader (BioTek) and the protein concentration of each sample was calculated based on the standard curve.

Sample preparation

Liver lysates from five animals in each intervention group were randomly picked for Western blot analyses. 100 µl lysate was mixed with 100 µl RIPA buffer containing a standard concentration of phosphatase- and protease -inhibitor (according to manufactures instructions). To spin down debris, the samples were centrifuged at 12000 rpm at 4°C in 15 minutes. The supernatant was pipetted into new microtubes and the pellet discarded. 30 µl of the sample was mixed with 82.5 µl RIPA buffer and 37.5 µl 4x Laemmli buffer (Sigma-Aldrich, MO, US) with DTT. The samples were heated at 95°C for five minutes, vortexed, and stored at -20°C.

SDS-polyacrylamide gel electrophoresis

SDS-polyacrylamide gel electrophoresis was run to separate the proteins based on their molecular weight. A Criterion™ TGX™ precast gel (Bio-Rad Laboratories, CA, US) with 4-20% acrylamide was placed in the Criterion™ Cell system (Bio-Rad Laboratories, CA, US). 1x running buffer (Appendix 3) was poured into the cell tank and each well flushed with the buffer to remove air bubbles. 10 µl sample containing 30 µg protein was loaded into each well. To be able to monitor the movement of the proteins and estimate their size, 3 µl of the Precision Plus Protein™ Prestained Standards (Bio-Rad Laboratories, CA, US) "dual ladder" and "all blue ladder", was loaded to the first and last well. The lid was placed on top of the tank prior to electrophoresis at 190 V for approximately 45 minutes.

Transfer

The proteins were transferred from the gel to a nitrocellulose membrane by semi-dry transfer using the "Trans-Blot® Turbo™ RTA Transfer Kit, Nitrocellulose" and the "Trans-

Blot® Turbo™ Transfer System" (Bio-Rad Laboratories, CA, US). The instructions from the manufacturer were followed, and a sandwich of paper-pad/gel/nitrocellulose-membrane/paper-pad was assembled in the transfer cassette. The current was set to 2.5 A for 7 or 10 minutes depending on whether proteins of interest had a low or high molecular weight, respectively.

Immunodetection

The membrane was first incubated at room temperature in a blocking buffer (5% BSA in TBS-T (Appendix 3)) with agitation to avoid non-specific binding of antibodies to the membrane. The blocking buffer was poured off after one hour, and primary antibody (Appendix 4) diluted in 2.5% BSA in TBS-T was added to the membrane before it was incubated overnight at 4°C with agitation. The next day, unbound primary antibody was removed by washing the membrane three times for 5-10 minutes in TBS-T. Then the washed membrane was incubated for one hour with agitation with HRP-conjugated secondary antibody diluted in 2.5% BSA in TBS-T. The membrane was washed in TBS-T as described above to remove unbound secondary antibody prior to immuno-detection.

The protein bands of interest were detected by the addition of a chemiluminescent HRP-substrate (SuperSignal® West Pico Chemiluminiscent Substrate (Thermo-Fisher Scientific, MA, US)). The emitted chemiluminescent light was imaged by the ChemiDoc™ Touch Imaging System (Bio-Rad Laboratories, CA, US). The intensities of protein bands in each lane were calculated using ImageJ software, by quantifying the areas under the curve for peaks after removal of background signal. The relative amount of the protein of interest in each lane was normalized against immunoblot signals for GAPDH for the same lane.

2.2.5 Analyses of liver tissue and plasma

Measurement of hepatic triglycerides content

Triglycerides were measured with Triglyceride (GPO) Reagent Set (Pointe Scientific Inc.). An aliquot of the liver lysate samples (see section 2.2.4) was diluted 30 times with MQ H_2O and vortexed. 16 µl of each dilute was pipetted onto a 96-well plate together with eight standards with decreasing concentrations of triglycerides (200 to 0 mg/dl). 200 µl of triglyceride (GPO) reagent was added to each well. After five minutes of incubation at room temperature, the absorbance was measured at 500 nm in the Synergy H1™ Hybrid Multi-

Mode Reader (BioTek). The absorbance levels of standards were used to create an 8-point standard curve that was used for calculation of triglyceride concentrations in the liver lysates.

Measurement of plasma triglycerides, cholesterol, and glucose

Colorimetric assays were used to determine plasma concentrations of TAG (Triglyceride (GPO) Reagent Set, Pointe Scientific Inc.), cholesterol (Cholesterol Reagent Set, Pointe Scientific Inc.), and glucose (Glucose (oxidase) Reagent Set, Pointe Scientific Inc.). Plasma samples were thawed on ice and diluted two times with MQ H_2O, prior to transfer of 5, 2.5 and 2 µl diluted plasma into three different 96-well plates for TAG, cholesterol and glucose measurements, respectively. Each plate contained eight standards with decreasing concentrations of TAG (200 to 0 mg/dl), cholesterol (200 to 0 mg/dl), or glucose (50 to 0 mM) which were added to the plate with the same volume as the plasma samples. 200 µl working reagent was pipetted into each well, followed by incubation according to the manufacturer's instructions. The absorbance for all assays was measured at 500 nm in the Synergy H1™ Hybrid Multi-Mode Reader (BioTek). The standards were used to create an 8-point standard curve that was used to determine the concentration of the unknown samples.

Measurement of plasma levels of alanine amino transferase

Pointe ALT (SGPT) Reagent Set (Pointe Scientific Inc.), was used for quantitative determination of alanine aminotransferase (ALT) in plasma. 10 and 5 µl plasma from MCS fed and MCD fed mice, respectively, were pipetted into a 96-well plate. 200 µl of preheated (37°C) working reagent were pipetted into each well before the plate was placed in the Synergy H1™ Hybrid Multi-Mode Reader (BioTek) with a program that measured absorbance at 340 nm after 1, 2 and 3 minutes in a temperature of 37°C. Calculations of ALT in IU/L plasma were performed as described in the manufacturer's instructions. In brief, the decline in absorbance was used to calculate the amount of ALT enzymes present in the plasma samples.

2.2.6 Statistical methods

All data presented are analysed in Microsoft excel 2016 (Microsoft®) and GraphPad Prism version 8 for Microsoft (GraphPad Software, San Diego, CA, US). Data are presented as means + standard error of the means (SEM). Two-way ANOVA followed by Holm-Sidak's

multiple comparisons test was performed using GraphPad Prism 8. The significance level was set to $p<0.05$.

3 Results

The accumulation of hepatocellular LDs is an important step in the pathophysiology of NAFLD. Plin family members are suggested to be important players during the disease progression as they serve as central regulators of LD metabolism (99). The existing research has mostly focused on the functions of Plin2 and Plin5, whereas no current research has investigated the role of Plin4 in the pathophysiology of NAFLD.

The goal of this master project was to study the role of Plin4 in the development of NASH. *Plin4*$^{+/+}$ and *Plin4*$^{-/-}$ mice were fed a methionine and choline deficient (MCD) diet to induce development of NASH. To assess the degree of liver damage caused by the MCD feeding, *Plin4*$^{+/+}$ and *Plin4*$^{-/-}$ mice were in parallel fed a control diet of equivalent nutritional composition but sufficient in methionine and choline (MCS).

The diet interventions and the collection of biological samples had been performed prior to the start of this master project. In this master project, differences in body- and organ-weights were analysed, and the collected biological materials were used to measure differences in metabolic plasma markers, hepatic content of TAG, and hepatic expression of selected genes and proteins. A detailed examination was performed on tissues from male mice since male mice have a faster and stronger response to dietary interventions that cause NAFLD compared to female mice (108, 109). Targeted analyses were also performed on tissues from female mice to look for sex differences in the progression towards NASH in *Plin4*$^{+/+}$ and *Plin4*$^{-/-}$ mice.

3.1.1 The effects of an MCD diet on body and organ weights

Analyses of mice characteristics were performed to determine if either the MCD diet or the absence of Plin4 affected body- and organ-weights. The following analyses included 20 *Plin4*$^{+/+}$ and 14 *Plin4*$^{-/-}$ male mice.

Mice fed the MCD diet showed a clear reduction in body- and organ-weights compared to the MCS fed mice, which likely was attributed to hypermetabolism, a reported effect of MCD feeding (110). This was an expected diet response, consistent with previous studies using the MCD model (110, 111), indicating that the diet intervention was successful. The absence of dietary methionine and choline resulted in a body weight loss of ~25% ($p<0.01$) (Fig. 3.1A), which mainly was caused by a reduction in adipose tissue mass, indicated by a ~55% weight reduction of epididymal- and inguinal fat depots in MCD fed

mice ($p<0.05$ and $p<0.01$, respectively) (Fig. 3.1C-D). MCD fed *Plin4*$^{-/-}$ mice had a significant reduction in liver weight mass of 29% ($p<0.01$), whereas a lower and nonsignificant reduction of 15% was found in *Plin4*$^{+/+}$ mice (Fig. 3.1B). Although the liver weight was reduced by MCD diet exposure, the liver to body weight ratio was not altered when compared to the MCS fed mice (Fig. 3.1G). The percentage weight loss in heart and kidneys in MCD fed mice were ~23% and ~28%, respectively ($p<0.01$) (Fig. 3.1E-F).

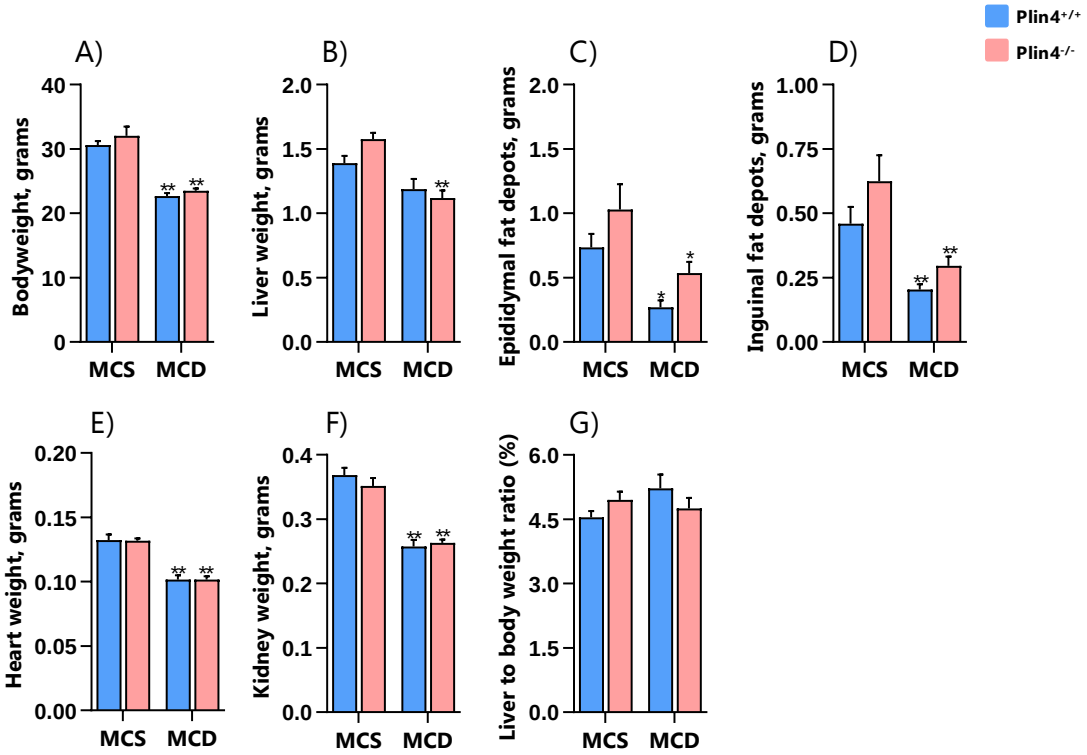

Figure 3.1: Methionine and choline deficiency resulted in reduced body- and organ weights: Male *Plin4*$^{+/+}$ and *Plin4*$^{-/-}$ mice were fed chow until 12 weeks of age, then given methionine and choline sufficient diet (MCS) for one week before mice were given MCS or methionine and choline deficient diet (MCD) for two additional weeks. Animal and organ weights for A) whole animal, B) liver, C), epididymal fat, D) subcutaneous fat in the inguinal area, E) heart, F) kidney, and G) liver relative to body weight. All data are presented as means + SEM. Differences between the two diets within the same genotype (*=$p<0.05$, **=$p<0.01$). n = 7-11 mice per group. Abbreviations used: MCS: Methionine and choline sufficient; MCD: Methionine and choline deficient.

3.1.2 The effect of MCD feeding on metabolic markers, hepatic steatosis, and liver damage

Mice fed the MCD diet lost a significant amount of adipose tissue weight. This indicates increased adipose tissue lipolysis, which is an expected effect of MCD feeding (112). To investigate metabolic consequences of the diet, metabolic plasma markers, hepatic TAG levels, and plasma ALT levels were measured.

MCD feeding led to a significant reduction of various metabolic plasma markers. Plasma TAG, total cholesterol, and glucose were reduced by 40 mg/dl, ($p<0.05$), 33 mg/dl, ($p<0.01$), and 5 mmol/L ($p<0.01$), respectively, in MCD fed *Plin4*$^{+/+}$ mice compared to MCS fed *Plin4*$^{+/+}$ mice (Fig. 3.2A-C). The observed reduced plasma TAG and cholesterol levels, suggests that decreased VLDL secretion contributes to the ~4-fold increase in hepatic TAG accumulation (Fig. 3.2D). Increased liver damage in MCD fed mice was indicated by an increase in plasma alanine aminotransferase (ALT) levels of ~124 IU/L ($p<0.01$) (Fig. 3.2E). There were no differences in these markers between *Plin4*$^{+/+}$ and *Plin4*$^{-/-}$ mice, implying that the MCD diet induced hepatic steatosis and liver damage to the same extent in *Plin4*$^{+/+}$ and *Plin4*$^{-/-}$ mice.

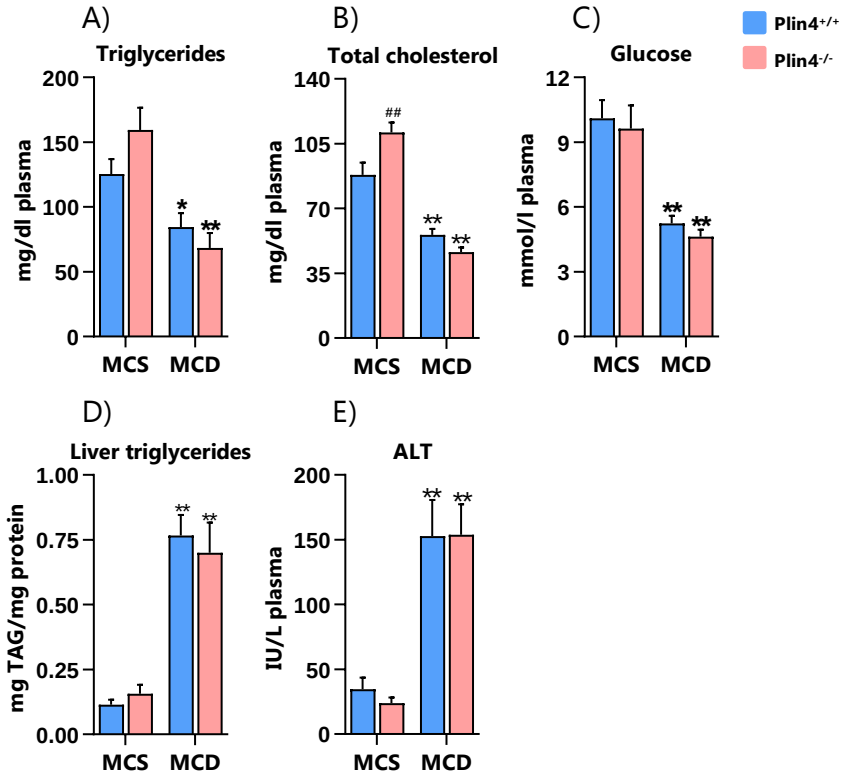

Figure 3.2: MCD feeding lowered metabolic plasma markers and induced hepatic steatosis and liver damage. Male *Plin4*$^{+/+}$ and *Plin4*$^{-/-}$ mice were fed as described in figure 3.1. Plasma and liver tissue analyses were conducted with colorimetric and enzymatic assays. A) plasma triglycerides, B) plasma total cholesterol, C) plasma glucose, D) liver triglycerides normalized against liver protein levels, and E) plasma alanine aminotransferase. All data are presented as means + SEM. Differences between the two diets within the same genotype (*=$p<0.05$, **=$p<0.01$), differences between *Plin4*$^{+/+}$ and *Plin4*$^{-/-}$ mice on the same diet (#=$p<0.05$, ##=$p<0.01$). n = 6-11 mice per group. Abbreviations used: ALT: Alanine aminotransferase; MCS: Methionine and choline sufficient; MCD: Methionine and choline deficient.

3.1.3 The effects of hepatic lipid accumulation on expression levels of genes related to lipid droplet metabolism

The previous data confirmed that the MCD diet induced hepatic lipid accumulation (See Fig. 3.2D). Excess lipids are normally sequestered in LDs. Therefore, expression of LD-binding genes was measured, to both investigate whether hepatic lipid accumulation altered their gene expression levels and if the absence of Plin4 was compensated for by an increased gene expression of other LD-binding proteins.

As expected, *Plin4*$^{-/-}$ mice had no detectable levels of *Plin4* mRNA (Fig. 3.3D). Of the Perilipin genes, *Plin3, Plin4* and *Plin5* were induced in MCD fed *Plin4*$^{+/+}$ mice (1.5-fold ($p<0.01$), 3.7-fold ($p<0.01$) and 1.8-fold ($p<0.01$), respectively, compared to MCS fed *Plin4*$^{+/+}$ mice ($p<0.01$)) (Fig. 3.3C-E). Expression of *Plin5* was not induced with the MCD diet in *Plin4*$^{-/-}$ mice, thus *Plin5* expression was lower in MCD fed *Plin4*$^{-/-}$ mice compared to *Plin4*$^{+/+}$ mice receiving the same diet ($p<0.01$) (Fig. 3.3E).

Gene expression levels were measured for other LD-binding proteins, such as the Cide-family members and proteins involved in lipolysis. Cide proteins are known to associate with LDs and regulate lipid metabolic pathways (113). The MCD fed mice showed no alteration in expression levels of *Cidea* and *Cideb,* but *Cidec* expression was increased more than 30-fold ($p<0.01$) (Fig. 3.3F-H). Expression levels of *G0s2, Abhd5,* and *Lipe* were not altered, but a 2-fold increase in *Pnpla2* expression was found in mice exposed to the MCD diet ($p<0.01$) (Fig. 3.3I-L).

The increased hepatic lipid accumulation in the MCD fed mice was followed by an elevated expression of several LD-binding proteins. However, the expression pattern was relatively similar between the *Plin4*$^{+/+}$ and *Plin4*$^{-/-}$ mice, except for the expression of *Plin5*.

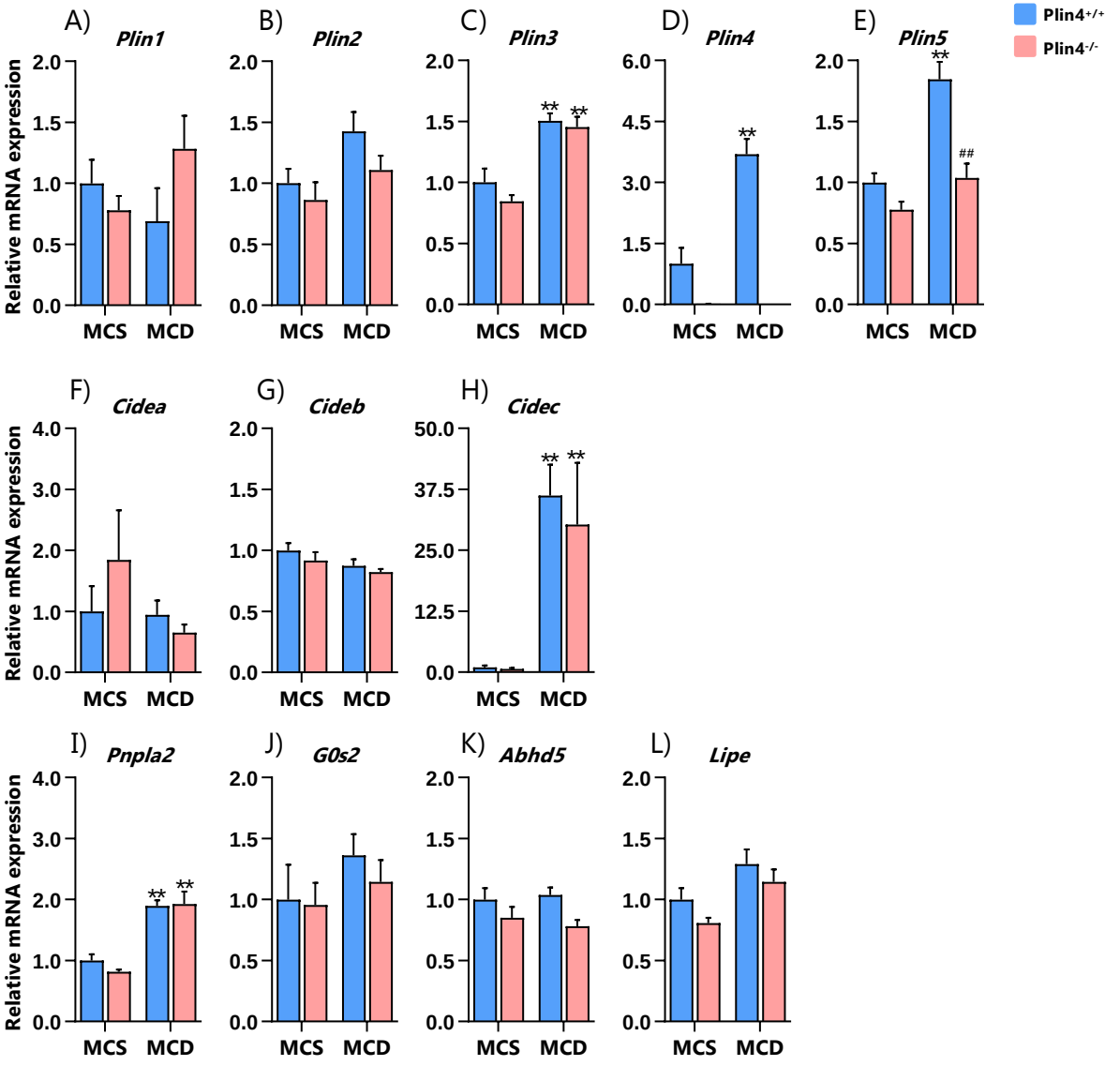

Figure 3.3: MCD feeding induced the hepatic expression of several genes related to lipid droplet binding. Male *Plin4*$^{+/+}$ and *Plin4*$^{-/-}$ mice were fed as described in figure 3.1. Gene expression levels for A) *Plin1*, B), *Plin2*, C) *Plin3*, D) *Plin4*, E) *Plin5*, F) *Cidea*, G) *Cideb*, H) *Cidec*, I) *Pnpla2*, J) *G0s2*, K) *Abhad5*, and L) *Lipe*. Gene expression levels were determined by RT-qPCR and were normalized to the expression of *Ppib*. The values are presented as the fold of the *Plin4*$^{+/+}$ mice fed the MCS diet. All data are presented as means + SEM. Differences between the two diets within the same genotype (*=p<0.05, **=p<0.01), differences between *Plin4*$^{+/+}$ and *Plin4*$^{-/-}$ mice on the same diet (#=p<0.05, ##=p<0.01). n = 7-9 mice per group. Abbreviations used: MCS: Methionine and choline sufficient; MCD: Methionine and choline deficient.

3.1.4 Hepatic expression of Perilipin proteins

The mRNA expression level for a gene does not necessarily correlate with the protein expression level (114). Hence immunoblotting of selected Plin proteins was conducted. MCD fed mice had increased hepatic expression of Plin2 and Plin5 (1.8-fold and 2.5-fold in *Plin4*$^{+/+}$ mice, respectively, compared to MCS fed *Plin4*$^{+/+}$ mice (p<0.01)) (Fig. 3.4B). In accordance with *Plin5* mRNA levels, expression of the Plin5 protein was not induced in the MCD fed

Plin4$^{-/-}$ mice. Expression of Plin5 was significantly lower in MCD fed *Plin4*$^{-/-}$ mice compared to *Plin4*$^{+/+}$ mice receiving the same diet ($p<0.01$) (Fig. 3.4B). The expression levels of Plin3 were stable and not influenced by MCD diet exposure (Fig. 3.4B). Based on these mRNA and protein analyses, it seems like the absence of Plin4 was not compensated for by increased expression of related Plin or Cide LD-binding proteins.

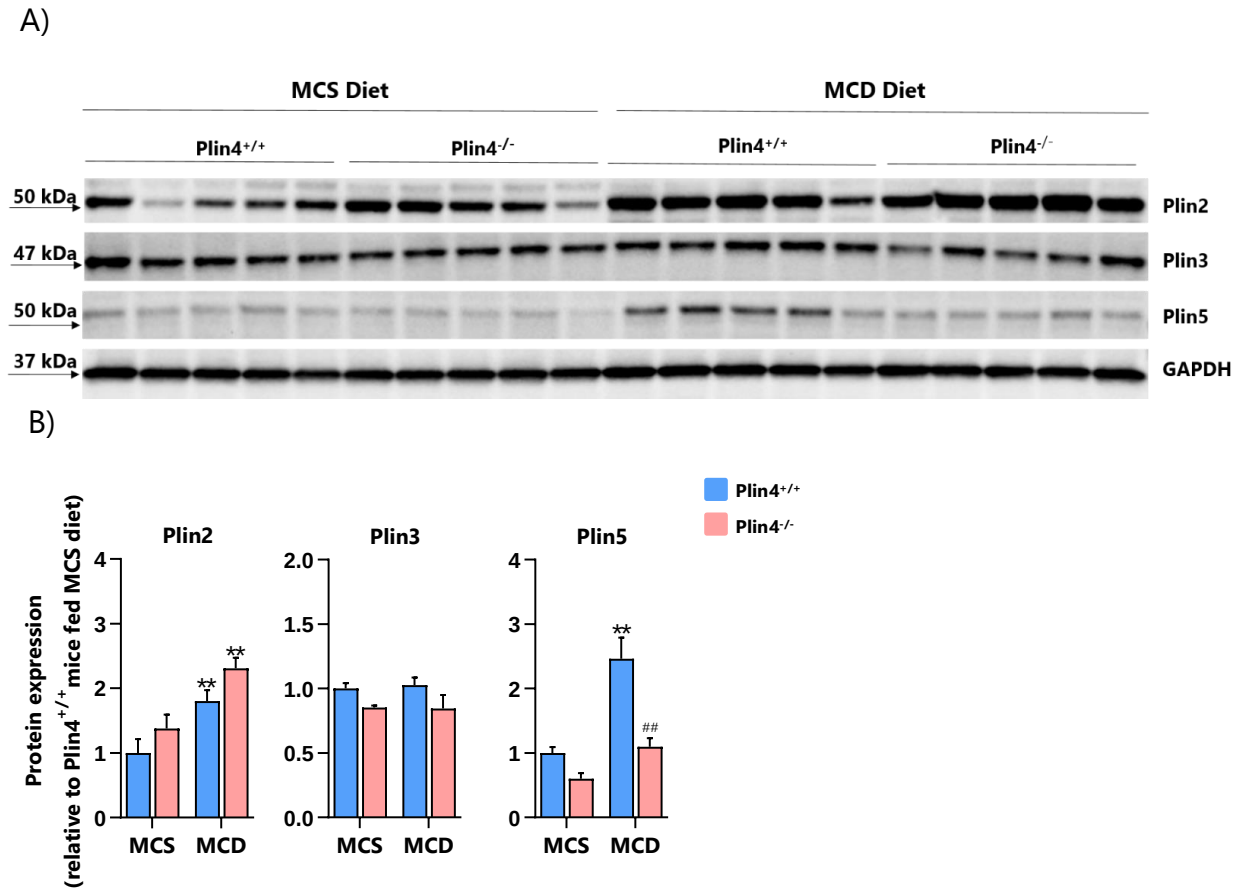

Figure 3.4: Hepatic expression of Perilipin proteins. Male *Plin4*$^{+/+}$ and *Plin4*$^{-/-}$ mice were fed as described in figure 3.1. **A)** Protein expression of Plin2, Plin3, Plin5, and GAPDH determined by Western blotting. 30 µg protein from five randomly selected liver lysates from each diet group were loaded. **B)** Plin2, Plin3 and Plin5 protein levels were normalized to GAPDH expression and presented relative to levels in MCS fed *Plin4*$^{+/+}$ mice. All data are presented as means + SEM. Differences between the two diets within the same genotype (*=$p<0.05$, **=$p<0.01$), differences between *Plin4*$^{+/+}$ and *Plin4*$^{-/-}$ mice on the same diet (#=$p<0.05$, ##=$p<0.01$). n = 5 mice per group. Abbreviations used: MCS: Methionine and choline sufficient; MCD: Methionine and choline deficient.

3.1.5 The effect of MCD feeding on hepatic expression of genes related to macrophages and inflammation

Next, we wanted to determine if the absence of Plin4 affected development of NASH. The hallmark of NASH is the presence of inflammation and hepatocyte injury (98). MCD fed mice had increased plasma levels of ALT (See Fig. 3.2E), suggesting that the diet induced

liver damage. Tissue damage triggers an immune response where inflammatory signalling molecules, such as interleukins and other cytokines, signal to recruit macrophages and other immune cells to the afflicted tissue. Hence, we measured hepatic expression of genes related to macrophages and inflammation.

Several genes related to macrophages and inflammation, including *Lyz* (7.5-fold, p<0.01), *Adgre* (3-fold, p<0.01), *Marco* (18.7-fold, p<0.01), *Il1b* (4.7-fold, p<0.01), *Il6* (3.7-fold, p<0.01), *Tnf* (12-fold, p<0.01), and *Dmpk* (2.7-fold, p<0.01) were induced in expression in MCD fed *Plin4*$^{+/+}$ mice compared to MCS fed *Plin4*$^{+/+}$ mice (Fig. 3.5A-G). This result indicates that the MCD diet led to development of NASH. Interestingly, the absence of Plin4 led to a blunted inflammatory gene expression in response to MCD feeding. Compared to MCD fed *Plin4*$^{+/+}$ mice, MCD fed *Plin4*$^{-/-}$ mice had significantly lower expression of *Lyz* (p<0.01), *Adgre* (p<0.05), *Il1b* (p<0.01), *Tnf* (p<0.01), and *Dmpk* (p<0.01) (Fig. 3.5A, B, D, F and G, respectively).

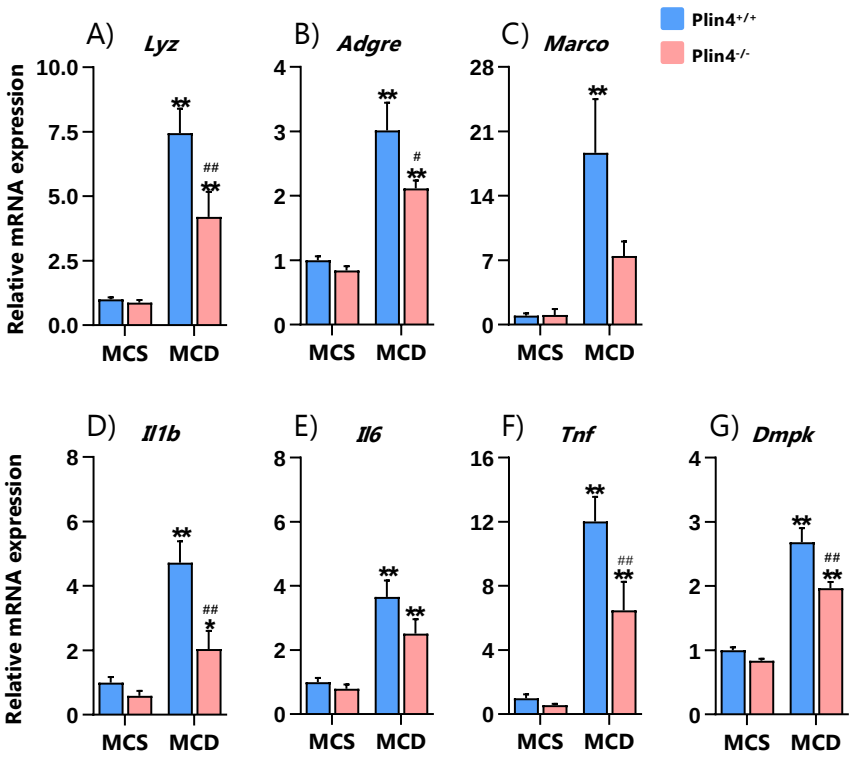

Figure 3.5: MCD feeding induced the hepatic expression of genes related to macrophages and inflammation, but to a lower extent in *Plin4*$^{-/-}$ male mice than in *Plin4*$^{+/+}$ male mice. Male *Plin4*$^{+/+}$ and *Plin4*$^{-/-}$ mice were fed as described in figure 3.1. Gene expression levels for A) *Lyz*, B) *Adgre*, C) *Marco*, D) *Il1b*, E) *Il6*, F) *Tnf*, and G) *Dmpk*. Gene expression levels were determined by RT-qPCR and were normalized to the expression of *Ppib*. The values are presented as the fold of the *Plin4*$^{+/+}$ mice fed the MCS diet. All data are presented as means + SEM. Differences between the two diets within the same genotype (*=p<0.05, **=p<0.01), differences between *Plin4*$^{+/+}$ and *Plin4*$^{-/-}$ mice on the same diet (#=p<0.05, ##=p<0.01). n = 7-9 mice per group. Abbreviations used: MCS: Methionine and choline sufficient; MCD: Methionine and choline deficient.

3.1.6 The effect of MCD feeding on hepatic expression of gene markers related to fibrosis and protein levels of α-SMA

Plin4$^{+/+}$ mice fed the MCD diet had higher gene expression levels of several genes related to macrophages and inflammation compared to *Plin4*$^{-/-}$ mice. To investigate if the difference in expression of inflammatory markers affected fibrosis development, genes related to fibrosis and hepatic protein expression of α-SMA were measured.

The MCD diet induced the expression of *Tgfb1* (2.9-fold) and *Col1a1* (5.5-fold) in MCD fed *Plin4*$^{+/+}$ mice compared to MCS fed *Plin4*$^{+/+}$ mice ($p<0.01$) (Fig. 3.6A-B). The same genes were induced in *Plin4*$^{-/-}$ mice, but expression of *Tgfb1* and *Col1a1* were lower in *Plin4*$^{-/-}$ mice compared to *Plin4*$^{+/+}$ mice receiving the MCD diet ($p<0.01$ and $p<0.05$, respectively) (Fig. 3.6A-B).

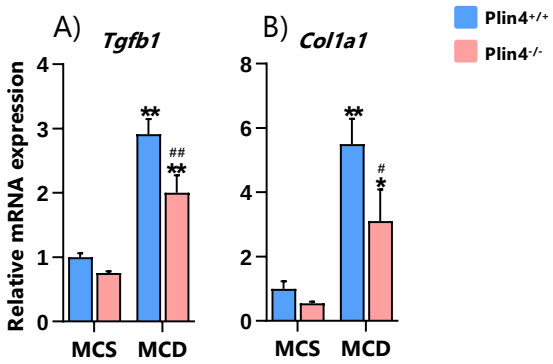

Figure 3.6: MCD feeding induced the hepatic expression of gene markers of fibrosis, but to a lower extent in *Plin4*$^{-/-}$ male mice than in *Plin4*$^{+/+}$ male mice. Male *Plin4*$^{+/+}$ and *Plin4*$^{-/-}$ mice were as described in figure 3.1. Gene expression levels for A) *Tgfb1*, and B) *Col1a1*. Gene expression levels were determined by RT-qPCR and were normalized to the expression of *Ppib*. The values are presented as the fold of the *Plin4*$^{+/+}$ mice fed the MCS diet. All data are presented as means + SEM. Differences between the two diets within the same genotype (*=$p<0.05$, **=$p<0.01$), differences between *Plin4*$^{+/+}$ and *Plin4*$^{-/-}$ mice on the same diet (#=$p<0.05$, ##=$p<0.01$). n = 7-9 mice per group. Abbreviations used: MCS: Methionine and choline sufficient; MCD: Methionine and choline deficient.

Transdifferentiation of hepatic stellate cells into fibrotic myofibroblasts is stimulated by TGF-β1 (encoded by the *Tgfb1 gene*), a central process in development of hepatic fibrosis (92). Since myofibroblasts are known to express high levels of α-SMA (92), hepatic α-SMA protein expression was measured. MCD fed *Plin4*$^{+/+}$ mice had a 3.3-fold increase in α-SMA expression compared to MCS fed *Plin4*$^{+/+}$ mice ($p<0.01$). No significant differences between *Plin4*$^{+/+}$ and *Plin4*$^{-/-}$ mice were found (Fig. 3.7B). Based on the mRNA markers and protein marker of fibrosis, it seems like two weeks of MCD feeding induced hepatic fibrosis development.

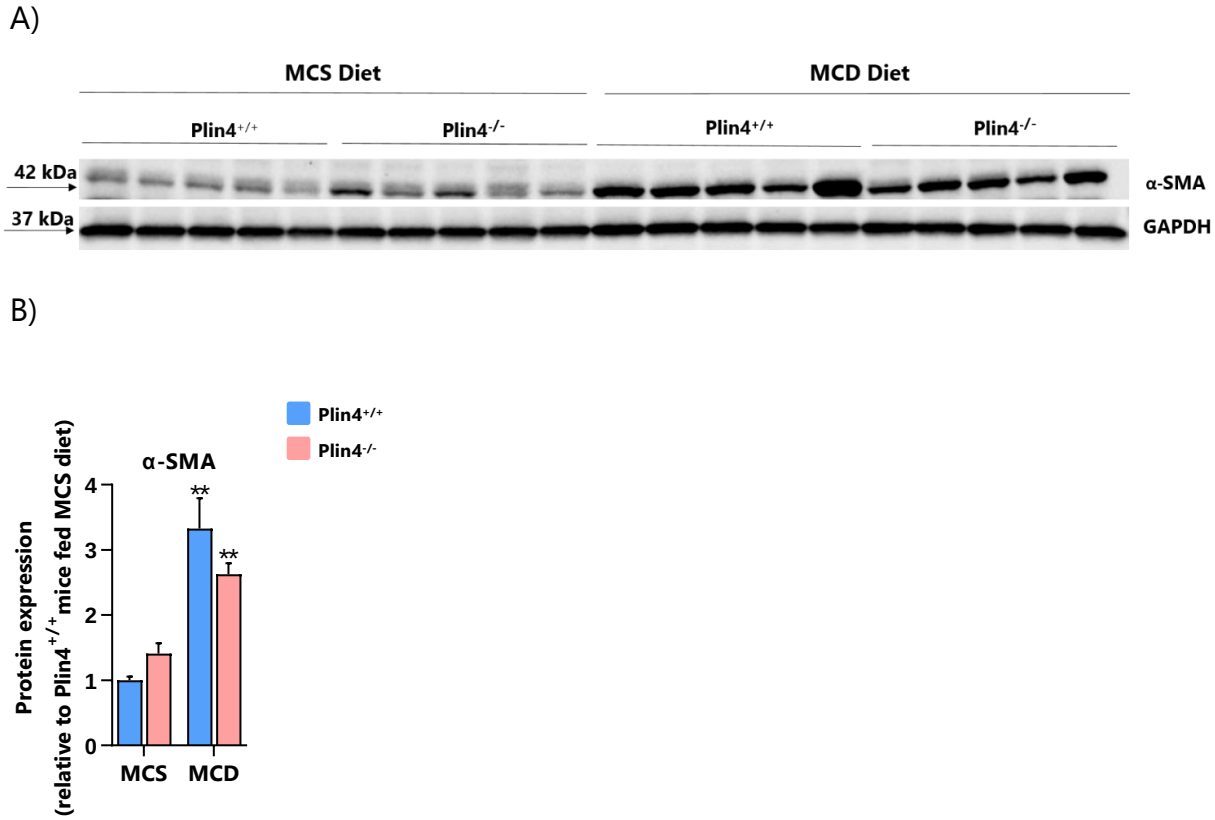

Figure 3.7: MCD feeding induced the hepatic expression of α-SMA. Male *Plin4*$^{+/+}$ and *Plin4*$^{-/-}$ mice were fed as described in figure 3.1. **A)** Protein expression of α-SMA and GAPDH determined by Western blotting. 30 µg protein from five randomly selected liver lysates from each diet group were loaded. **B)** α-SMA protein levels were normalized to GAPDH expression and presented relative to levels in MCS fed *Plin4*$^{+/+}$ mice. All data are presented as means + SEM. Differences between the two diets within the same genotype (*=p<0.05, **=p<0.01). n = 5 mice per group. Abbreviations used: α-SMA: alpha smooth muscle actin; MCS: Methionine and choline sufficient; MCD: Methionine and choline deficient.

3.1.7 The effect of MCD feeding on hepatic expression of genes involved in *de novo* lipogenesis

To look for an explanation for the differences in development of NASH between *Plin4*$^{+/+}$ and *Plin4*$^{-/-}$ mice, genes important for hepatic lipid metabolism were analysed. FAs synthesized from *de novo* lipogenesis are an important source for the TAG accumulated in steatotic livers (86). To investigate the activity of hepatic *de novo* lipogenesis, expression levels of central lipogenic TFs and some of their downstream genes were measured.

MCD fed *Plin4*$^{+/+}$ mice had reduced expression levels of the lipogenic TFs *Srebf1c* and *Chrebpa* with a fold reduction of 48% and 27%, respectively, compared to MCS fed *Plin4*$^{+/+}$ mice ($p<0.01$) (Fig. 3.8B-D). *Plin4*$^{+/+}$ mice exposed to the MCD diet had a 1.3-fold increase in *Srebf1a* expression ($p<0.01$), whereas the expression level remained unchanged in *Plin4*$^{-/-}$ mice receiving the same diet (Fig. 3.8A). While mRNA expression of the lipogenic

rate limiting *Acaca* remained unchanged, the enzyme catalysing synthesis of fatty acids, *Fasn*, was induced ~2-fold ($p<0.05$ or $p<0.01$) in MCD fed mice compared to MCS fed *Plin4*$^{+/+}$ mice (Fig. 3.8E-F).

Overall, the MCD diet appeared to reduce or not affect the expression of lipogenic TFs when compared to the MCS diet. There was no clear association between expression of the typical lipogenic TFs and the induction of the lipogenic enzyme *Fas*. The absence of *Plin4* appeared to have negligible effects on gene expression levels of the lipogenesis-related genes studied.

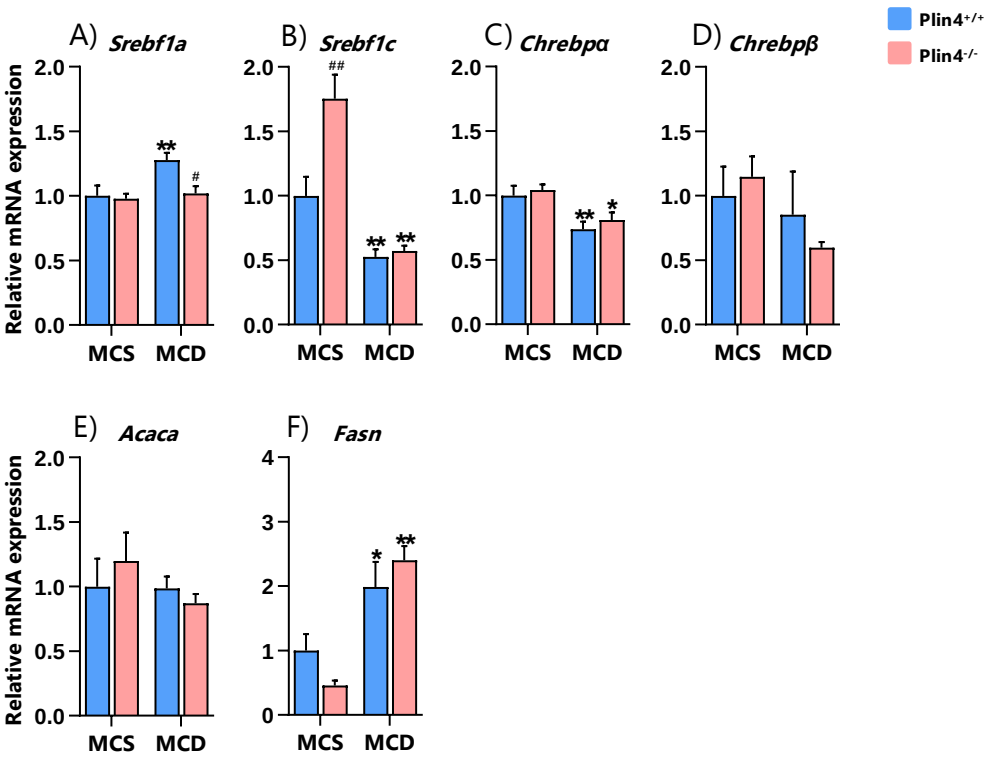

Figure 3.8: Hepatic expression of genes involved in lipogenesis. Male *Plin4*$^{+/+}$ and *Plin4*$^{-/-}$ mice were fed as described in figure 3.1. Gene expression levels for A) *Srebf1a*, B) *Srebf1c*, C) *Chrebpa* D) *Chrebpβ,* E) *Acaca*, and F) *Fasn*. Gene expression levels were determined by RT-qPCR and were normalized to the expression of *Ppib*. The values are presented as the fold of the *Plin4*$^{+/+}$ mice fed the MCS diet. All data are presented as means + SEM. Differences between the two diets within the same genotype (*=$p<0.05$, **=$p<0.01$), differences between *Plin4*$^{+/+}$ and *Plin4*$^{-/-}$ mice on the same diet (#=$p<0.05$, ##=$p<0.01$). n = 7-9 mice per group. Abbreviations used: MCS: Methionine and choline sufficient; MCD: Methionine and choline deficient.

3.1.8 The effect of MCD feeding on hepatic expression of genes involved in fatty acid metabolism

To determine if fatty acid sensors or fatty acid degradation were different in MCD fed *Plin4*$^{+/+}$ and *Plin4*$^{-/-}$ mice, a few key genes involved in catabolism of fatty acids were measured. PPARs are central regulators of lipid metabolism and are activated upon ligand

binding, mainly by various FAs (37). Activated PPARs regulate activation of various downstream genes, such as *Cpt1a* and *Acox1* (37), which encodes the two central β-oxidation enzymes CPT1A and ACOX1, respectively.

The MCD diet induced expression of *Ppara* by 1.3-fold in *Plin4*$^{-/-}$ mice ($p<0.05$), whereas the expression was unaltered in *Plin4*$^{+/+}$ mice (Fig. 3.9A). MCD diet decreased *Ppard* expression by 52% in *Plin4*$^{+/+}$ mice ($p<0.01$), while *Pparg* expression increased 3-fold ($p<0.01$), when compared to MCS fed *Plin4*$^{+/+}$ mice (Fig. 3.9B-C). The expression of *Cpt1a* and *Acox1* was increased by 60% ($p<0.01$) and decreased by 40% ($p<0.05$), respectively, in MCD fed *Plin4*$^{+/+}$ mice compared to MCS fed *Plin4*$^{+/+}$ mice (Fig. 3.9D-E). Although the induction in *Cpt1a* expression indicates that transport of FAs into the mitochondria may be increased, lowered expression levels of the PPARα target gene, *Acox1*, suggest that PPARα activity and β-oxidation may be reduced in *Plin4*$^{+/+}$ and *Plin4*$^{-/-}$ mice receiving the MCD diet.

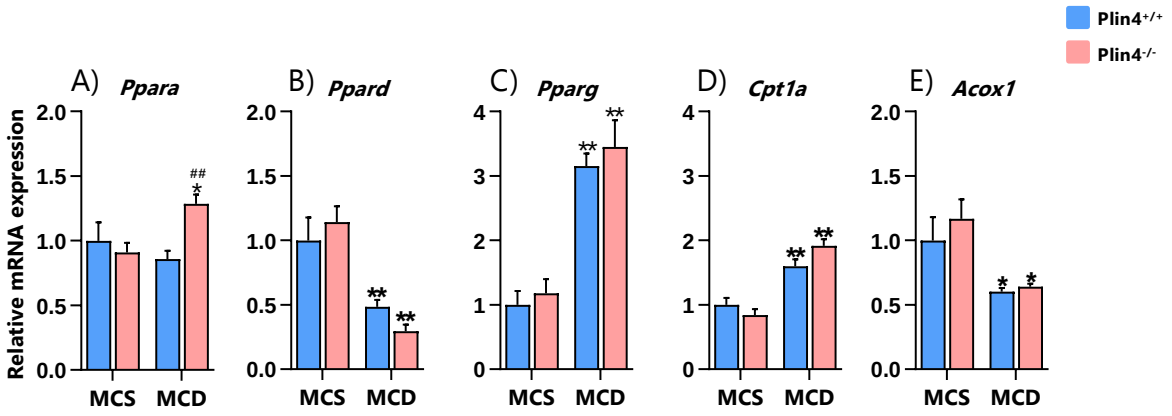

Figure 3.9: Hepatic expression of genes involved in fatty acid metabolism. Male *Plin4*$^{+/+}$ and *Plin4*$^{-/-}$ mice were fed as described in figure 3.1. Gene expression levels for A) *Ppara*, B) *Ppard*, C) *Pparg*, D) *Cpt1a*, and E) *Acox1*. Gene expression levels were determined by RT-qPCR and were normalized to the expression of *Ppib*. The values are presented as the fold of the *Plin4*$^{+/+}$ mice fed the MCS diet. All data are presented as means + SEM. Differences between the two diets within the same genotype (*=$p<0.05$, **=$p<0.01$), differences between *Plin4*$^{+/+}$ and *Plin4*$^{-/-}$ mice on the same diet (#=$p<0.05$, ##=$p<0.01$). n = 7-9 mice per group. Abbreviations used: MCS: Methionine and choline sufficient; MCD: Methionine and choline deficient.

3.2 Female mice

To determine if differences in the expression of macrophage, inflammation and fibrosis markers found in MCD fed *Plin4*$^{+/+}$ and *Plin4*$^{-/-}$ male mice also occurred in female mice, the same analyses were performed on samples from *Plin4*$^{+/+}$ and *Plin4*$^{-/-}$ female mice receiving an MCS or an MCD diet.

3.2.1 The effects of an MCD diet on body and organ weights

The analyses of female mice included 18 *Plin4*$^{+/+}$ mice and 20 *Plin4*$^{-/-}$ mice. MCD diet exposure reduced body- and organ-weights in female mice, similar to what was observed in male mice. The absence of dietary methionine and choline resulted in a body weight loss of ~23% (Fig. 3.10A). The percentage weight loss of liver, periovarian- and inguinal -fat depots, heart, and kidneys were 14%, 46%, 29%, 20%, and 27%, respectively, in MCD fed *Plin4*$^{+/+}$ mice (Fig. 3.10B-F). Essentially the same reductions were observed in the MCD fed *Plin4*$^{-/-}$ mice. The liver to body weight was significantly increased in mice receiving the MCD diet ($p<0.05$) (Fig. 3.10G).

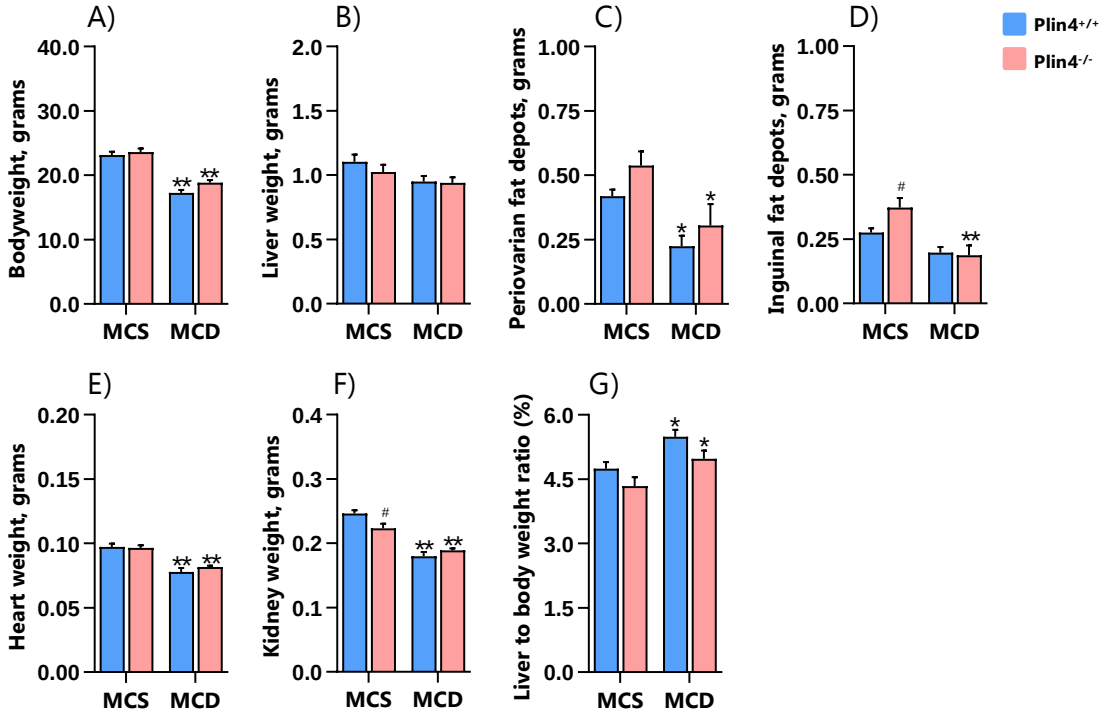

Figure 3.10: Methionine and choline deficiency resulted in reduced body- and organ-weights: Female *Plin4*$^{+/+}$ and *Plin4*$^{-/-}$ mice were fed chow until 12 weeks of age, then given methionine and choline sufficient diet (MCS) for one week before mice were given MCS or methionine and choline deficient diet (MCD) for two additional weeks. Animal and organ weights for A) whole animal, B) liver, C), periovarian fat, D) subcutaneous fat in the inguinal area, E) heart, F) kidney, and G) liver relative to body weight. All data are presented as means + SEM. Differences between the two diets within the same genotype (*=$p<0.05$, **=$p<0.01$), differences between *Plin4*$^{+/+}$ and *Plin4*$^{-/-}$ mice on the same diet (#=$p<0.05$, ##=$p<0.01$). In *Plin4*$^{-/-}$ mice receiving the MCD diet, data on periovarian and inguinal fat depots weight were only collected from 4 mice. n=4-11 mice per group. Abbreviations used: MCS: Methionine and choline sufficient; MCD: Methionine and choline deficient.

3.2.2 The effect of MCD feeding on hepatic expression of genes related to lipid droplet metabolism

Expression of a few of the LD-binding proteins that were altered by MCD diet in male mice were measured to investigate whether the same gene regulatory alterations occurred in female mice. As expected, *Plin4* mRNA was not detected in *Plin4*$^{-/-}$ mice (Fig. 3.11A). *Plin4*, *Plin5* and *Cidec* were induced in MCD fed *Plin4*$^{+/+}$ mice (18.6-fold ($p<0.01$), 2.1-fold ($p<0.01$), and 77.8-fold ($p<0.01$), respectively, compared to MCS fed *Plin4*$^{+/+}$ mice) (Fig. 3.11A-C). Female *Plin4*$^{-/-}$ mice receiving the MCD diet did also induce *Plin5* expression ($p<0.01$), but the expression of *Plin5* was significantly lower compared to *Plin4*$^{+/+}$ mice receiving the same diet ($p<0.01$) (Fig. 3.11B). Overall, the MCD diet caused similar gene alterations in female and male mice, with female mice showing an even higher induction of *Plin4* and *Cidec* mRNA expression.

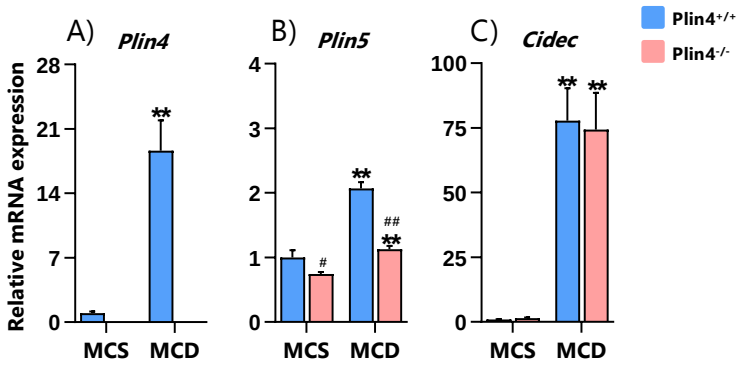

Figure 3.11: Dietary lack of methionine and choline induced the expression of genes encoding lipid droplet binding proteins. Female *Plin4*$^{+/+}$ and *Plin4*$^{-/-}$ mice were fed as described in figure 3.10. Gene expression levels for A) *Plin4*, B) *Plin5*, and G) *Cidec*. Gene expression levels were determined by RT-qPCR and were normalized to the expression of *Ppib*. The values are presented as the fold of the *Plin4*$^{+/+}$ mice fed the MCS diet. All data are presented as means + SEM. Differences between the two diets within the same genotype (*=$p<0.05$, **=$p<0.01$), differences between *Plin4*$^{+/+}$ and *Plin4*$^{-/-}$ mice on the same diet (#=$p<0.05$, ##=$p<0.01$). n=9-11 mice per group. Abbreviations used: MCS: Methionine and choline sufficient; MCD: Methionine and choline deficient.

3.2.3 The effect of MCD feeding on hepatic expression of genes related to macrophages, inflammation and fibrosis

MCD fed male mice had an increased expression of several genes related to macrophages, inflammation, and fibrosis. The same genes, including *Lyz* (3.2-fold, $p<0.01$), *Marco* (5.5-fold, $p<0.01$), *Il1b* (4.5-fold, $p<0.01$), *Tnf* (7.7-fold, $p<0.01$), and *Col1a1* (3.5-fold, $p<0.01$) were induced in MCD fed female *Plin4*$^{+/+}$ mice compared to MCS fed female *Plin4*$^{+/+}$ mice (Fig. 3.12A-E). Similar expression patterns were observed in *Plin4*$^{-/-}$ female

mice. In contrast to male mice, a statistically significant difference between MCD fed female *Plin4*$^{-/-}$ and *Plin4*$^{+/+}$ mice was only found for *Tnf* ($p<0.05$) (Fig. 3.12D), with only a tendency towards a weaker fold induction compared to *Plin4*$^{+/+}$ mice for the other measured genes. These results indicate that the MCD diet led to increased hepatic inflammation and macrophage infiltration in female mice, but with an overall weaker fold induction of the measured genes compared to male mice. This suggests that NASH develops at a slower rate by MCD feeding in female mice than in male mice.

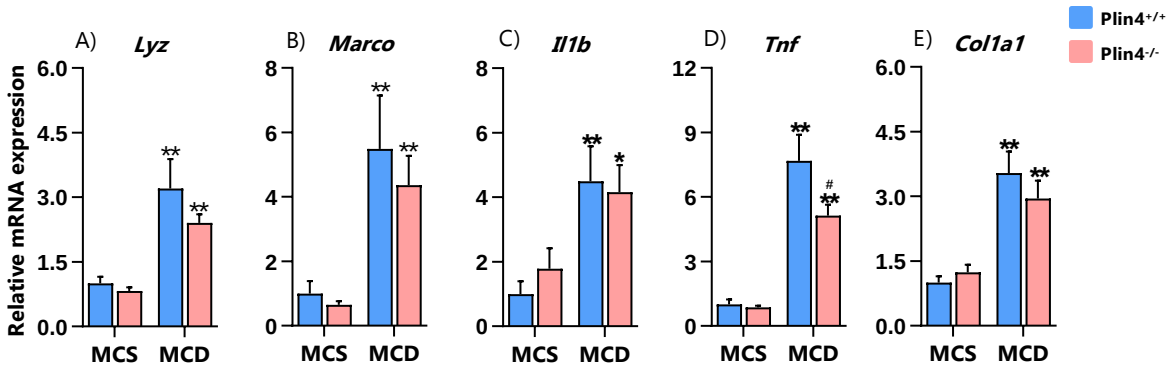

Figure 3.12: Methionine and choline deficiency induced the hepatic expression of genes related to macrophages, inflammation, and fibrosis in female mice, but the fold induction was overall lower than in male mice. Female *Plin4*$^{+/+}$ and *Plin4*$^{-/-}$ mice were fed as described in figure 3.10. Gene expression levels of A) *Lyz*, B) *Marco*, C) *Il1b*, D) *Tnf*, and E) *Col1a1*. Gene expression levels were determined by RT-qPCR and were normalized to the expression of *Ppib*. The values are presented as the fold of the *Plin4*$^{+/+}$ mice fed the MCS diet. All data are presented as means + SEM. Differences between the two diets within the same genotype (*=$p<0.05$, **=$p<0.01$), differences between *Plin4*$^{+/+}$ and *Plin4*$^{-/-}$ mice on the same diet (#=$p<0.05$, ##=$p<0.01$). n=9-11 mice per group. Abbreviations used: MCS: Methionine and choline sufficient; MCD: Methionine and choline deficient.

4 Discussion

4.1 Discussion of the methodology

4.1.1 Mice as a model system to study human diseases

The laboratory mouse has a high genetic and physiological similarity to humans and is a widely used organism to study human biology and disease (115). In experimental animal research, it is common to use an inbred mouse strain where all individuals have the same genetic background. This reduces genetic diversity in the study population, which will lower experimental variation. When animals are housed in the same highly controlled environment, all individuals are expected to respond nearly identical to a treatment. With a reduced variance in exposure responses, a small study population will be needed to investigate the biological effects of an intervention. However, it is important to remember that the measured effects do not necessarily reflect the response for mice as a species in nature, which will have high genetic diversity and be exposed to different environments.

Laboratory mouse studies are carried out under strictly controlled conditions. Mice are housed in cages in specially dedicated rooms that makes it possible to control their environment closely, such as food availability, temperature, humidity, light/dark cycle, and the presence of pathogens. This reduces the presence of confounding factors and makes it possible to study the effect of an experimental intervention with a low number of animals per treatment group.

Even though mice studies are a cost-efficient way to study human biology, discrepancies between the two species imply that obtained results are not necessarily transferable to humans.

The *Plin4* knockout mouse model

To study the role of Plin4 in the development of NASH, *Plin4* knockout mice were generated with homologous recombination in 129/Sv embryonic stem (ES) cells, a commonly used method for gene disruption. A congenic strain of *Plin4*$^{-/-}$ mice in the CB7BL/6N background was created by backcrossing the genetically modified mice for more than ten generations (Dalen, K.T., unpublished results). In this master project, the genotypes were validated by the presence or absence of *Plin4* mRNA by RT-qPCR. None of the *Plin4*$^{-/-}$ mice had detectable levels of *Plin4* mRNA.

The *Plin4*$^{+/+}$ and *Plin4*$^{-/-}$ mice studied were from the same breeding colony and were therefore genetically identical except for the presence or absence of *Plin4*. A weakness in the female mice study was that the MCS diet intervention was completed two years after the MCD diet intervention. Importantly, numerous feeding studies performed by the research group since 2014 have documented high experimental reproducibility. Because the same inbred strain has been used and the breeding conditions have been unaltered in this period, this gap in time is expected to have minor effects on the results.

4.1.2 Dietary models for NAFLD development

Because of the rising prevalence of NAFLD in humans, various animal models have become important research tools to investigate the disease's pathophysiology in order to identify safe and effective therapeutic targets (116). There are various dietary models to induce NAFLD in mice, but none that mimics the entire pathogenesis spectrum found in humans (83). The MCD diet, high-fat high-sucrose/fructose (Western) diets, and various high-fat (HF) diets are commonly used (83, 94). The MCD diet is known for its rapid induction of a NASH phenotype in mice. After two weeks of feeding, mild NASH develops, accompanied by prominent hepatic steatosis, increased inflammation, and recruitment of inflammatory cells (111, 117), that further progresses to severe NASH at week eight (94) with manifestation of hepatic fibrosis at week 10 (111). This makes the MCD diet a valuable model for studying the inflammatory and fibrotic elements of NASH (94). A disadvantage with this model is that the disease manifestation is restricted to the hepatic tissue. The extrahepatic metabolic changes that are present in NAFLD patients, such as obesity and insulin resistance, are thus not reflected (83). These disease aspects are better mimicked by the other dietary models such as Western- and HF-diets. However, such diets require a much longer feeding period in order to cause a more progressive form of NAFLD. Only mild NASH develops after ~16 weeks of Western diet feeding (94, 118), while advanced NASH with fibrosis develops after 52 weeks (119). HF diet feeding for ~16 weeks induces hepatic steatosis without hepatocyte injury and inflammation (118, 120). After 80 weeks of feeding, most aspects of the pathophysiology of human NASH, such as obesity, IR, and hepatic inflammation, and fibrosis development, are mimicked (121). Such feeding studies are, therefore, compared to the MCD diet, very time-consuming and expensive to perform.

Although the MCD diet has its limitations, it is considered a suitable model to study the mechanisms behind NASH development (94, 98). MCD diet is a fast approach to screen

for candidate genes and mechanisms, and hence we used the MCD dietary model to determine if Plin4 plays a role in steatosis and the development of NASH. To minimize the stress for the animals, the MCD diet was given for only two weeks, which should be sufficient to detect differences in inflammation markers that indicate development of NASH. If the experiments revealed a potential role for Plin4 in the development of NASH, the research group intends to perform other feeding studies using dietary models that better reflect the natural disease spectrum of human NAFLD.

4.1.3 Quantitative reverse transcription polymerase chain reaction

RT-qPCR is an efficient, fast, reproducible, and highly sensitive method to study gene expression levels, where even weakly expressed genes can be quantified (122, 123). The technique was used in this master project to compare the expression of genes related to lipid metabolism, inflammation, and fibrosis in *Plin4*$^{+/+}$ and *Plin4*$^{-/-}$ mice fed either the MCS or the MCD diet. The preparation of samples for RT-qPCR and the RT-qPCR method itself includes several steps which need to be performed with high precision to generate reliable results.

To produce cDNA of high quality, the isolated RNA must be pure and free of contaminants, such as DNA, proteins, guanidine, and phenols. Particularly phenol but also other substances introduced during the RNA extraction steps can inhibit the reaction steps of cDNA synthesis and qPCR. This affects the final quantitative gene expression analysis. The phenol-chloroform extraction step and the addition of a high salt solution were added to the purification steps in the NucleoSpin RNA kit (Macherey-Nagel, Düren, Germany) to increase the purity of the isolated RNA. To minimize DNA contamination, the RNA samples did also undergo a DNase treatment step. The quantity and purity of each isolated RNA sample was determined by the Nano Drop ND-1000 spectrophotometer (Thermo Scientific, Waltham, MA). The RNA used for cDNA synthesis was therefore confirmed to be of high purity, and if not, the sample was isolated again prior to cDNA synthesis.

The fluorescence dye, SYBR Green, was used as a reporter assay to detect the amounts of double stranded DNA amplicons generated in each PCR cycle. A disadvantage with SYBR Green is that it intercalates non-specifically with dsDNA, which may cause an overestimation of the gene of interest if more than one target sequence is amplified or if the sample is contaminated with DNA. With this in mind, it was important to avoid contamination of the samples during preparation and to use primer pairs with high specificity to their target gene in order to avoid synthesis of non-specific amplicons.

This disadvantage with SYBR Green can be circumvented by replacing it with a probe-based reporter system, such as TaqMan probes. Reporter probes are designed to specifically bind to the target sequence of interest in the region between the two primers that are used to amplify the target region. This design ensures that fluorophore signals only are generated from the gene of interest and thus increase the specificity of the method. However, since each measured gene needs a well-designed specific probe, this method is more expensive compared to the SYBR Green reporter assay. To verify the absence of fluorescence signals from non-specific dsDNA and primer dimers, when using SYBR Green, a melt curve was run and two negative controls were included for each gene expression assay.

The relative quantification of gene expression levels was obtained by normalizing the qPCR data for each target gene against the expression of a reference gene. Hence, it was of great importance to search for an appropriate reference gene that was not affected by the experimental factors to achieve reliable results. Housekeeping genes (HKG) are commonly used reference genes. They are normally expressed at a steady and constant level in every cell of an organism since the genes are needed to maintain basal cellular functions (123, 124). The expression of several HKG was measured, of which *Ppib* was selected as an appropriate reference gene due to its stable expression among the intervention groups.

To determine whether the mRNA levels corresponded with its encoding protein, Western blot analyses were performed for some of the measured genes. Western blotting is a semi-quantitative technique. Thus, the quantified protein levels were used for relative comparison between the intervention groups.

4.1.4 Missing analyses

The hepatic expression of the Plin4 protein was not reported in this master thesis. Several attempts were made to obtain a Western blot of hepatic Plin4 expression, but none succeeded. This included different methods of preparing the samples, the use of alternative dry and wet transfer techniques, and the use of different Plin4 antibodies. Samples from gonadal fat depots from *Plin4*$^{+/+}$ and *Plin4*$^{-/-}$ mice were included as positive and negative controls on Western blots, respectively. Immunoblot of the adipose tissue samples showed clear Plin4 bands in the *Plin4*$^{+/+}$ mice, whereas the same bands were not detected in the *Plin4*$^{-/-}$ mice (Figure in appendix 5). This experiment confirmed that the antibody worked, suggesting that protein expression of Plin4 in hepatic tissue might be too low to be detected by Western blotting.

4.1.5 Statistical methods

Differences between groups were tested with Two-way ANOVA followed by Holm-Sidak's multiple comparisons test. The Two-way ANOVA is a parametric test that assumes that the data is normally distributed, that the variance of the groups is equal, and that the observations are independent of each other (125). The small sample size (7-11 mice in each intervention group) made it difficult to determine whether the data were normally distributed or not. This because normality tests have little power in small sample sizes (126) and visual assessments of normal distribution are difficult to interpret based on few samples.

For some of the genes related to macrophages and inflammation, there was doubt as to whether the genes were normally distributed. These genes were additionally analysed with the non-parametric Mann-Whitney test. The statistical results were similar to the results gained from parametric testing. Therefore, we decided to use the same statistical method on all the results presented in this master thesis.

4.2 Discussion of the results

The pathogenesis of NASH is complex, involving hepatic lipid accumulation, followed by increased inflammation and fibrosis (14). Hepatic lipid accumulation is characterized by excessive deposition of hepatocellular LDs, which has linked LD metabolism and its associated proteins to the pathogenesis of NAFLD (99). Several studies have used *Plin* knock-out/knock-down models to understand the involvement of Plins in NAFLD (102-105), but currently, no studies have explored the role of Plin4, which was the primary goal of this master project.

In this master project, 13 weeks old *Plin4*$^{+/+}$ and *Plin4*$^{-/-}$ mice were fed an MCD diet for two weeks to develop hepatosteatosis with progression towards NASH. MCD feeding led to increased liver TAG accumulation, elevated plasma ALT levels, induced hepatic protein expression of α-SMA, and increased hepatic expression of genes related to inflammation and fibrosis. These results demonstrate that the MCD-diet intervention was successful. The absence of Plin4 in male mice fed an MCD diet did not affect body- and organ-weights, hepatic TAG accumulation, plasma levels of ALT, or hepatic protein expression of α-SMA, but consistently did alleviate hepatic induction of gene markers related to inflammation and fibrosis. The molecular explanation behind the mitigated inflammatory response to MCD feeding in male *Plin4*$^{-/-}$ mice is unknown, but as will be discussed later, we speculate that some of the effects could be mediated through differences in *Plin5* and *Ppara* expression

levels. MCD diet also seemed to cause inflammation in female mice, but the effect was weaker, which might have masked a difference between *Plin4*$^{+/+}$ and *Plin4*$^{-/-}$ mice in this gender.

4.2.1 Consequences of methionine and choline deficiency on hepatic triglyceride accumulation and lipid droplet morphology

Enhanced hepatic uptake of FAs, originating from adipose tissue lipolysis, and decreased secretion of VLDL particles, are two important mechanisms for hepatic TAG accumulation in the MCD model (127). The effect on VLDL secretion is a consequence of the reduced availability of methionine and choline for PC biosynthesis, which is required for normal hepatic secretion of VLDL particles (95, 96). We showed that MCD fed mice had reduced plasma levels of TAG and cholesterol, which may be attributed to decreased hepatic VLDL secretion. Further, we found that MCD feeding increased hepatic TAG accumulation. We found no differences in hepatic steatosis between *Plin4*$^{+/+}$ and *Plin4*$^{-/-}$ mice, suggesting that Plin4 likely does not affect hepatic TAG accumulation. This differs from rodent studies on mice with an absence of Plin2, Plin3, or Plin5, which all were found to have reduced hepatic steatosis in dietary models of NAFLD (102-105, 128).

As well as being essential for VLDL secretion, PC is a crucial component of LDs. PC is the most abundant phospholipid in the LD membrane where it plays an important role in preventing LDs from coalescence (47, 52). The reduced availability of PC in MCD fed mice may therefore have altered the size and stability of the accumulated LDs. We did not examine histologically whether the LD morphology was altered in the absence of Plin4. This would have been interesting to analyse, since the alpha-helix of Plin4 is found to directly coat and stabilize neutral lipids, implying that Plin4 may function as a substitution for phospholipids (56, 129). Therefore, we speculate if the induced expression of *Plin4* in the MCD fed *Plin4*$^{+/+}$ mice may have served as a replacement for insufficient availability of PC for LD synthesis and expansion. Furthermore, overexpression of the Plin4 alpha-helix has been shown to reduce the LD size in cultured S2 cells with impaired PC production when compared to similar cells without expression of the Plin4 alpha-helix (56). This may suggest that the hepatocellular LDs in *Plin4*$^{+/+}$ mice were smaller compared to *Plin4*$^{-/-}$ mice. Future studies that use the MCD model to investigate the role of Plin4 in the development of NASH should therefore include a histological assessment of hepatic tissue to determine whether the hepatic LD morphology is altered in the absence of Plin4.

4.2.2 MCD feeding induces hepatic expression of *Plin4*

We showed that MCD feeding significantly induced the expression of *Plin4* in *Plin4*$^{+/+}$ mice. Others have shown that HF- and Western-diet feeding upregulates the hepatic expression of *Plin4* in rodents (130, 131). *Plin4* is suggested to be weakly expressed in the liver (65). Our failure to identify hepatic Plin4 proteins supports this observation and indicates that Plin4 starts to be of importance when the liver starts to accumulate lipids. This is analogous to the other Plin family members, which also are shown to be upregulated in steatotic livers (100-103). The significant rise in *Pparg* expression found in the MCD fed mice was a likely mediator of the induced *Plin4* expression since *Plin4* is a direct target gene of *Pparg* in other tissues (62). The increased expression of *Pparg* could have been a consequence of hepatic macrophage infiltration, as activated macrophages have high expression of *Pparg* (37), and therefore presumably likely also express *Plin4*. We therefore speculate whether the increased hepatic *Plin4* expression partly was a cause of elevated levels of macrophages in the hepatic tissue of MCD fed mice. To understand the induction of *Plin4*, it would be interesting to identify hepatic cell types that express *Plin4* when mice are exposed to an MCD diet, or alternatively, in other models of NASH.

4.2.3 *Plin4*$^{-/-}$ mice on an MCD diet had attenuated induction of inflammatory and fibrosis markers

The primary finding of this study was an attenuated inflammatory response to MCD feeding in male mice when Plin4 was absent. We showed that male *Plin4*$^{-/-}$ mice had a significantly lower induction of several genes related to macrophages, inflammation, and fibrosis compared to male *Plin4*$^{+/+}$ mice after two weeks on an MCD diet. This is a novel finding that indicates that Plin4 is involved in the inflammatory aspects of NAFLD progression and suggests that the absence of Plin4 may slow the progression towards NASH development. The biological significance of the finding is still unknown and warrants further investigation.

The finding discussed above is based on differences in gene expression levels. We did not confirm whether the same differences were present at protein level, neither did we perform a histological assessment to investigate whether hepatic infiltration of immune cells and fibrosis development correlated with the genotype differences in gene expression levels. Such analyses would have strengthened our observed gene expression data.

Previous studies have revealed potential roles of other Plin family members in NAFLD. Liver-specific loss of Plin2 alleviates hepatic lipid accumulation, inflammation, and fibrosis induced by MCD feeding (104). Absence of Plin5 reduces hepatic TAG accumulation but is found to both increase and reduce hepatic liver injury in mouse models of NAFLD (102, 105). Reduction in Plin3 expression reduces hepatic TAG accumulation and improves glucose tolerance in mice fed an HF diet (103), but it is unclear if Plin3 plays a role in NAFLD. So far, studies have suggested that Plin2 and Plin5 may be potential therapeutic targets for NAFLD. According to our findings, the same may also apply to Plin4.

4.2.4 Absence of Plin4 reduces Plin5 mRNA and protein expression

The absence of a gene may be compensated for by an increased expression of alternative genes with similar functions. However, our findings demonstrate that absence of Plin4 does not result in any compensating upregulated gene or protein expression of related Plin family members. On the contrary, we showed that *Plin4*$^{-/-}$ mice failed to induce hepatic Plin5 mRNA and protein expression when fed the MCD diet. This is consistent with a previous study by Chen et al., demonstrating that *Plin4*$^{-/-}$ mice have reduced gene and protein expression of Plin5 in heart, white adipose tissue, and the liver (65). Since the genes encoding Plin5 and Plin4 are located next to each other in the genome, the researchers were concerned that their intended deletion of *Plin4* unintendedly altered transcriptional regulatory elements that affected expression of the *Plin5* gene (65). Since we now see similar effects on Plin5 expression in the absence of Plin4, this seems less likely. In addition, *Plin5* deletion has not been shown to affect Plin4 mRNA or protein expression (102). How the absence of Plin4 influences the expression of *Plin5* is still an unanswered question that needs further investigation.

Plin5 is an important hepatic LD binding protein. Hence, the attenuated inflammatory response to MCD feeding found in *Plin4*$^{-/-}$ male mice can potentially be explained by their lack of Plin5 induction. However, studies investigating the role of Plin5 in NAFLD and NASH are ambiguous. Asimakopoulos et al. showed that *Plin5*$^{-/-}$ mice fed an HF diet for 30 weeks had an alleviated induction of pro-inflammatory gene markers and were protected against liver injury, shown by no rise in serum levels of liver damage enzymes (105). This study supports that the absence of Plin5 may protect against development of NASH, which potentially can explain the alleviated inflammatory response to MCD feeding we found in the *Plin4*$^{-/-}$ male mice. However, findings from Wang et al. suggest rather a protective role of

Plin5 in NAFLD. They found that *Plin5*$^{-/-}$ mice fed an HF diet had elevated hepatic lipolysis that increased the levels of FFAs in the liver. This was accompanied by hepatic inflammation and lipotoxic injury caused by lipid peroxidation of FFAs (102). As a support to a protective role of Plin5, another study reported that expression of Plin5 prevents inflammation during fasting (132). The findings of these studies are thus ambiguous, and additional detailed studies in *Plin5*$^{-/-}$ mice are needed to clarify the role of Plin5 in NAFLD and NASH development. Regardless of the role of Plin5, two studies have reported reduced hepatic steatosis in *Plin5*$^{-/-}$ mice when fed a diet that induces NAFLD (102, 105). We did not observe any differences in liver TAG accumulation between *Plin4*$^{+/+}$ and *Plin4*$^{-/-}$ male mice, although there were significant differences in Plin5 expression levels. It is therefore not possible to determine if the different inflammatory response to MCD feeding between *Plin4*$^{-/-}$ and *Plin4*$^{+/+}$ male mice was caused by a direct effect of Plin4 absence and insufficient coating of hepatic LDs, or alternatively were mediated through downregulation of Plin5.

4.2.5 Methionine and choline deficiency induced *Ppara* expression in *Plin4*$^{-/-}$ male mice

We found that the expression of *Ppara* was significantly induced in MCD fed *Plin4*$^{-/-}$ male mice, whereas it remained stable in the *Plin4*$^{+/+}$ male mice. *Ppara* expression is found to correlate negatively with NASH severity in liver tissue samples from patients with NAFLD/NASH (133). Additionally, rodent studies have shown that mice with absence of PPARα have increased liver inflammation and an accelerated NAFLD progression when fed an HF diet (134, 135). This suggest that PPARα is important in NAFLD progression, which made us speculate whether the induced expression of *Ppara* in *Plin4*$^{-/-}$ mice could explain their alleviated inflammatory response to MCD feeding.

However, the PPARα transcription factor needs to be activated by ligand binding to perform its functions, and it is unclear if PPARα activity was altered upon MCD feeding or absence of Plin4. We found no differences in expression levels of the two measured downstream genes of PPARα; *Cpt1a* and *Acox1*, between *Plin4*$^{+/+}$ and *Plin4*$^{-/-}$ male mice. Although significant differences in *Ppara* expression were found between MCD fed *Plin4*$^{+/+}$ and *Plin4*$^{-/-}$ male mice, the similarly reduced levels of *Acox1* expression after MCD diet suggest that the activity of PPARα was reduced. The PC species 16:0/18:1-GPC is suggested to be an important hepatic endogenous ligand for PPARα (136). Deficiency in methionine and

choline is expected to result in reduced synthesis of PC (95), which may explain why activation of PPARα is mitigated in the livers of MCD fed mice.

4.2.6 Gender differences in NAFLD/NASH susceptibility

In our study, we showed that MCD fed female mice had upregulated expression of genes related to inflammation and fibrosis, but the fold induction was overall lower compared to MCD fed male mice. This finding is in agreement with previous research on gender differences in NASH susceptibility. MCD feeding is known to induce a more severe liver injury in males compared to female rodents (137), with a higher degree of hepatic steatosis and plasma ALT levels, and a higher induction of inflammatory mediator genes (138). Similar gender differences are also found when using other dietary models, such as long-term feeding with Western diets and HF diets (108, 109).

In humans, the prevalence of NAFLD is higher in men than in women (139, 140), but interestingly, the prevalence is considerably higher in postmenopausal women compared to men and premenopausal women (141). The reduction in oestrogen levels following menopause is thought to be the cause of increased susceptibility to NAFLD in postmenopausal women (141). The reduction in oestrogen makes the women more prone to weight gain, abdominal fat accumulation, and insulin resistance, factors that are associated with NAFLD (141). A role of oestrogen in NAFLD development is also shown in rodents. Kamada et al. found that female mice with oestrogen deficiency have enhanced liver injury with faster progression towards NASH when exposed to high-fat and high-cholesterol feeding, which could be improved with oestrogen therapy (142). This suggests a protective role of oestrogen in NAFLD progression.

Our MCD interventions in both sexes is in agreement with other previous research suggesting that female mice have a slower progression towards NASH compared to male mice. Female mice require a longer feeding period to develop the same degree of liver injury as found in the male mice. Due to this difference in response, male mice seem more optimal to use in experiments that investigate the role of Plins in NASH development. However, it is important to perform studies in both sexes to discover gender differences.

5 Conclusion

In this study, we demonstrated that the absence of Plin4 seems to protect against hepatic inflammation and development of NASH. This was demonstrated by an attenuated induction of several genes related to inflammation and fibrosis in *Plin4*$^{-/-}$ male mice compared to *Plin4*$^{+/+}$ male mice receiving an MCD diet. This is a novel finding that warrants further investigation to explain the molecular background behind the effect. Future studies should examine whether the same differences in inflammatory and fibrotic gene markers are present at the protein level and include a histological assessment to investigate whether the absence of Plin4 also results in less hepatic immune cell infiltration and fibrosis development. In future experiments, a more natural diet for development of NASH should be used. Such a study will be needed to clarify if the absence of Plin4 has the same effects in a model that better mimics the human features of NAFLD.

Our study observed that absence of Plin4 did not affect hepatic TAG accumulation, but we do not know whether the lipid droplet morphology was altered. Lipid droplet sizes and their lipid species should be investigated in future experiments, as previous findings suggest that the alpha-helix of Plin4 can stabilize neutral lipids and function as a substitution for phospholipids (56, 129). Without such analyses, one can only speculate whether the induced expression of *Plin4* compensates for reduced availability of PC for LD synthesis and expansion in MCD fed *Plin4*$^{+/+}$ mice.

Our study demonstrated that the absence of Plin4 reduces the hepatic expression of Plin5 on both the mRNA and protein level in mice receiving an MCD diet. Others have shown the same with other diets (65), indicating that there is a relationship between Plin4 and the expression of Plin5, but the molecular explanation behind the effect is still unclear and warrants further research.

Our study demonstrated that MCD fed female mice have a slower progression towards NASH compared to male mice. The attenuated response to MCD feeding in female mice may explain why we did not detect the same genotype differences in gene markers of NASH as were observed in male mice. Future MCD-feeding experiments using female mice should therefore last longer to be able to investigate if absence of Plin4 also alleviates the inflammatory and fibrotic effects of MCD feeding in females. The stronger response to dietary interventions that cause development of NASH in males suggests that male mice are

more optimal to use in experiments that investigate the role of Plins in NASH. However, it is important to perform studies in both sexes to discover gender differences.

With the increasing prevalence of NAFLD, the need of developing safe and effective therapeutic targets is urgent. Manipulation of Plin expression or binding of Plins to the LD surface seems like a potential therapeutic strategy. In this study, we demonstrated that absence of Plin4 may attenuate development of NASH by alleviating the expression of inflammatory and fibrotic gene markers. The biological mechanism involved is still unknown, necessitating the need for more research to fully understand the role of Plin4 (and other Plin proteins) in NAFLD.

References

1. Ng M, Fleming T, Robinson M, Thomson B, Graetz N, Margono C, et al. Global, regional, and national prevalence of overweight and obesity in children and adults during 1980–2013: a systematic analysis for the Global Burden of Disease Study 2013. Lancet. 2014;384(9945):766-81.
2. Bleich S, Cutler D, Murray C, Adams A. Why Is the Developed World Obese? Annu Rev Public Health. 2008;29(1):273-95.
3. Hruby A, Hruby A, Hu FB, Hu FB. The Epidemiology of Obesity: A Big Picture. PharmacoEconomics. 2015;33(7):673-89.
4. Fabbrini E, Sullivan S, Klein S. Obesity and nonalcoholic fatty liver disease: Biochemical, metabolic, and clinical implications. Hepatology. 2010;51(2):679-89.
5. Giskes K, van Lenthe F, Brug J. A systematic review of environmental factors and obesogenic dietary intakes among adults: are we getting closer to understanding obesogenic environments? Obes Rev. 2011;12(501):e95-e106.
6. Chooi YC, Ding C, Magkos F. The epidemiology of obesity. Metabolism. 2019;92:6-10.
7. World Health Organization. Obesity and overweight [Internet]. [Updated 1. April 2020; cited 28. March 2021] Available from: https://www.who.int/news-room/fact-sheets/detail/obesity-and-overweight.
8. Nevill AM, Stewart AD, Olds T, Holder R. Relationship between adiposity and body size reveals limitations of BMI. Am J Phys Anthropol. 2006;129(1):151-6.
9. Hu FB. Obesity and Mortality: Watch Your Waist, Not Just Your Weight. Arch Intern Med. 2007;167(9):875-6.
10. Castro AV, Kolka CM, Kim SP, Bergman RN. Obesity, insulin resistance and comorbidities? Mechanisms of association. Arq Bras Endocrinol Metabol. 2014;58(6):600-9.
11. Janssen I, Heymsfield SB, Allison DB, Kotler DP, Ross R. Body mass index and waist circumference independently contribute to the prediction of nonabdominal, abdominal subcutaneous, and visceral fat. Am J Clin Nutr. 2002;75(4):683-8.
12. Midthjell K, Lee CMY, Langhammer A, Krokstad S, Holmen TL, Hveem K, et al. Trends in overweight and obesity over 22 years in a large adult population: the HUNT Study, Norway. Clinical obesity. 2013;3(1-2):12-20.
13. Ibrahim MM. Subcutaneous and visceral adipose tissue: structural and functional differences. Obes Rev. 2010;11(1):11-8.
14. Arab JP, Arrese M, Trauner M. Recent Insights into the Pathogenesis of Nonalcoholic Fatty Liver Disease. Annu Rev Pathol. 2018;13(1):321-50.
15. Samuel VT, Shulman GI. Nonalcoholic Fatty Liver Disease as a Nexus of Metabolic and Hepatic Diseases. Cell Metab. 2018;27(1):22-41.
16. Holck P. Leveren [Internet] Store medisinske leksikon; [Updated 12. May 2020; cited 22. April 2021]. Available from: https://sml.snl.no/leveren.
17. Abdel-Misih SR, Bloomston M. Liver Anatomy. Surg Clin North Am. 2010;90(4):643-53.
18. Rogers AB, Dintzis RZ. Hepatobiliary System. I: Piper M, editor. Comparative Anatomy and Histology; Second Edition. Academic Press; 2018. p. 229-239.
19. Suchy FJ. Hepatobilary Function: I: Boron WF, Boulpaep EL, editor. Medical Physiology, Third Edition. Elsevier; 2017. p. 944-971.
20. Rui L. Energy Metabolism in the Liver. Compr Physiol. 2011;4(1):177-97.

21. Frayn KN. Digestion and Intestinal Absorption. Metabolic regulation: A human perspective, Third Edition. Malden, USA: Blackwell; 2010. p. 53-76 ed. ed.
22. Han HS, Kang G, Kim JS, Choi BH, Koo SH. Regulation of glucose metabolism from a liver-centric perspective. Exp Mol Med. 2016;48(3):e218.
23. Ferrier DR. The Feed-Fast Cycle. Lippincott's illustrated reviews: Biochemistry, Seventh Edition. Philadelphia: Wolters Kluwer; 2017. p. 321-36.
24. Sanders FW, Griffin JL. De novo lipogenesis in the liver in health and disease: more than just a shunting yard for glucose. Biol Rev Camb Philos Soc. 2016;91(2):452-68.
25. Zhang D, Yin L. Transcriptional Regulation of De Novo Lipogenesis in Liver. I: Ntambi JM, ed. Cham: Springer International Publishing; 2016. p. 1-31.
26. Hardy T, Oakley F, Anstee QM, Day CP. Nonalcoholic Fatty Liver Disease: Pathogenesis and Disease Spectrum. Annu Rev Pathol. 2016;11(1):451-96.
27. Kersten S. Mechanisms of nutritional and hormonal regulation of lipogenesis. EMBO Rep. 2001;2(4):282-6.
28. Wang Y, Viscarra J, Kim SJ, Sul HS. Transcriptional regulation of hepatic lipogenesis. Nat Rev Mol Cell Biol. 2015;16(11):678-89.
29. Duncan RE, Ahmadian M, Jaworski K, Sarkadi-Nagy E, Sul HS. Regulation of lipolysis in adipocytes. Annu Rev Nutr. 2007;27(1):79-101.
30. Lafontan M, Langin D. Lipolysis and lipid mobilization in human adipose tissue. Prog Lipid Res. 2009;48(5):275-97.
31. Ahmadian M, Wang Y, Sul HS. Lipolysis in adipocytes. Int J Biochem Cell Biol. 2010;42(5):555-9.
32. Schulz H. Oxidation of fatty acids in eukaryotes. I: Vance DE, Vance JE, ed. Biochemistry of Lipids, Lipoproteins and Membranes, Fifth Edition. Elsevier; 2008. p. 131-154.
33. Ferrier DR. Fatty Acid, Triacylglycerol, and Ketone Body Metabolism. Lippincott's illustrated reviews: Biochemistry, Seventh Edition. Philadelphia: Wolters Kluwer; 2017. p. 181-200.
34. Schreurs M, Kuipers F, van der Leij FR. Regulatory enzymes of mitochondrial beta-oxidation as targets for treatment of the metabolic syndrome. Obes Rev. 2010;11(5):380-8.
35. Sugden MC, Caton PW, Holness MJ. Peroxisome Proliferator-Activated Receptors. I: Lennarz WJ, Lane MD, ed. Encyclopedia of Biological Chemistry, Second Edition. Waltham: Elsevier; 2004. p. 239-245.
36. Zardi EM, Navarini L, Sambataro G, Piccinni P, Sambataro FM, Spina C, et al. Hepatic PPARs: their role in liver physiology, fibrosis and treatment. Curr Med Chem. 2013;20(27):3370-96.
37. Wang Y, Nakajima T, Gonzalez FJ, Tanaka N. PPARs as Metabolic Regulators in the Liver: Lessons from Liver-Specific PPAR-Null Mice. Int J Mol Sci. 2020;21(6):2061.
38. Kersten S, Stienstra R. The role and regulation of the peroxisome proliferator activated receptor alpha in human liver. Biochimie. 2017;136:75-84.
39. Francis GA, Fayard E, Picard F, Auwerx J. Nuclear receptors and the control of metabolism. Annu Rev Physiol. 2003;65(1):261-311.
40. Zandbergen F, Plutzky J. PPARα in atherosclerosis and inflammation. Biochim Biophys Acta. 2007;1771(8):972-82.
41. Olzmann JA, Carvalho P. Dynamics and functions of lipid droplets. Nat Rev Mol Cell Biol. 2019;20(3):137-55.
42. Walther TC, Chung J, Farese RV. Lipid Droplet Biogenesis. Annu Rev Cell Dev Biol. 2017;33(1):491-510.

43. Sztalryd C, Brasaemle DL. The perilipin family of lipid droplet proteins: Gatekeepers of intracellular lipolysis. Biochim Biophys Acta Mol Cell Biol Lipids. 2017;1862(10):1221-32.
44. Walther TC, Farese RV. Lipid Droplets and Cellular Lipid Metabolism. Annu Rev Biochem. 2012;81(1):687-714.
45. Kimmel AR, Sztalryd C. The Perilipins: Major Cytosolic Lipid Droplet-Associated Proteins and Their Roles in Cellular Lipid Storage, Mobilization, and Systemic Homeostasis. Annu Rev Nutr. 2016;36(1):471-509.
46. Xu S, Zhang X, Liu P. Lipid droplet proteins and metabolic diseases. Biochim Biophys Acta Mol Basis Dis. 2018;1864(5):1968-83.
47. Thiam AR, Farese JRV, Walther TC. The biophysics and cell biology of lipid droplets. Nat Rev Mol Cell Biol. 2013;14(12):775-86.
48. Sharma M, Mitnala S, Vishnubhotla RK, Mukherjee R, Reddy DN, Rao PN. The Riddle of Nonalcoholic Fatty Liver Disease: Progression From Nonalcoholic Fatty Liver to Nonalcoholic Steatohepatitis. J Clin Exp Hepatol. 2015;5(2):147-58.
49. Farese RV, Walther TC. Lipid Droplets Finally Get a Little R-E-S-P-E-C-T. Cell. 2009;139(5):855-60.
50. Itabe H, Yamaguchi T, Nimura S, Sasabe N. Perilipins: a diversity of intracellular lipid droplet proteins. Lipids Health Dis. 2017;16(1):83.
51. Cohen S. Lipid Droplets as Organelles. Int Rev Cell Mol Biol. 2018;337:83-110.
52. Krahmer N, Guo Y, Wilfling F, Hilger M, Lingrell S, Heger K, et al. Phosphatidylcholine Synthesis for Lipid Droplet Expansion Is Mediated by Localized Activation of CTP:Phosphocholine Cytidylyltransferase. Cell Metab. 2011;14(4):504-15.
53. Farese RV, Walther TC. Lipid Droplets Finally Get a Little R-E-S-P-E-C-T. Cell. 2009;139(5):855-60. Figure 1. Anatomy of a Lipid Droplet p. 856.
54. Kimmel AR, Brasaemle DL, McAndrews-Hill M, Sztalryd C, Londos C. Adoption of PERILIPIN as a unifying nomenclature for the mammalian PAT-family of intracellular lipid storage droplet proteins. J Lipid Res. 2010;51(3):468-71.
55. Bickel PE, Tansey JT, Welte MA. PAT proteins, an ancient family of lipid droplet proteins that regulate cellular lipid stores. Biochimica et biophysica acta Molecular and cell biology of lipids. 2009;1791(6):419-40.
56. Čopič A, Antoine-Bally S, Giménez-Andrés M, La Torre Garay C, Antonny B, Manni MM, et al. A giant amphipathic helix from a perilipin that is adapted for coating lipid droplets. Nat Commun. 2018;9(1):1332.
57. Rowe ER, Mimmack ML, Barbosa AD, Haider A, Isaac I, Ouberai MM, et al. Conserved Amphipathic Helices Mediate Lipid Droplet Targeting of Perilipins 1–3. J Biol Chem. 2016;291(13):6664-78.
58. Londos C, Sztalryd C, Tansey JT, Kimmel AR. Role of PAT proteins in lipid metabolism. Biochimie. 2005;87(1):45-9.
59. Tansey JT, Sztalryd C, Gruia-Gray J, Roush DL, Zee JV, Gavrilova O, et al. Perilipin Ablation Results in a Lean Mouse with Aberrant Adipocyte Lipolysis, Enhanced Leptin Production, and Resistance to Diet-Induced Obesity. Proc Natl Acad Sci U S A. 2001;98(11):6494-9.
60. Kimmel AR, Sztalryd C. Perilipin 5, a lipid droplet protein adapted to mitochondrial energy utilization. Curr Opin Lipidol. 2014;25(2):110-7.
61. Dalen KT, Dahl T, Holter E, Arntsen B, Londos C, Sztalryd C, et al. LSDP5 is a PAT protein specifically expressed in fatty acid oxidizing tissues. Biochimica et biophysica acta Molecular and cell biology of lipids. 2007;1771(2):210-27.
62. Dalen KT, Schoonjans K, Ulven SM, Weedon-Fekjaer MS, Bentzen TG, Koutnikova H, et al. Adipose Tissue Expression of the Lipid Droplet–Associating Proteins S3-12 and

Perilipin Is Controlled by Peroxisome Proliferator–Activated Receptor-γ. Diabetes. 2004;53(5):1243-52.
63. Nathan EW, James RS, Marissa JS, Anatoly T, Kenneth GB, Perry EB. Adipocyte Protein S3-12 Coats Nascent Lipid Droplets. J Biol Chem. 2003;278(39):37713-21.
64. Hsieh K, Lee YK, Londos C, Raaka BM, Dalen KT, Kimmel AR. Perilipin family members preferentially sequester to either triacylglycerol-specific or cholesteryl-ester-specific intracellular lipid storage droplets. J Cell Sci. 2012;125(Pt 17):4067-76.
65. Weiqin C, Benny C, Xinyu W, Lan L, Mark S, Lawrence C. Inactivation of Plin4 downregulates Plin5 and reduces cardiac lipid accumulation in mice. Am J Physiol Endocrinol Metab. 2013;304(7):770-9.
66. Calzadilla Berlot-L, Adams LA. The Natural Course of Non-Alcoholic Fatty Liver Disease. Int J Mol Sci. 2016;17(5):774.
67. Liu K, McCaughan GW. Epidemiology and Etiologic Associations of Non-alcoholic Fatty Liver Disease and Associated HCC. Adv Exp Med Biol. 2018;1061:3-18.
68. Naveed S, Ewan F, David P. Non-alcoholic fatty liver disease. BMJ. 2014;349:4596-g.
69. Ong JP, Younossi ZM. Epidemiology and Natural History of NAFLD and NASH. Clin Liver Dis. 2007;11(1):1-16.
70. Verma S, Jensen D, Hart J, Mohanty SR. Predictive value of ALT levels for non-alcoholic steatohepatitis (NASH) and advanced fibrosis in non-alcoholic fatty liver disease (NAFLD). Liver Int. 2013;33(9):1398-405.
71. Sheka AC, Adeyi O, Thompson J, Hameed B, Crawford PA, Ikramuddin S. Nonalcoholic Steatohepatitis: A Review. JAMA. 2020;323(12):1175-83.
72. Ge X, Zheng L, Wang M, Du Y, Jiang J. Prevalence trends in non-alcoholic fatty liver disease at the global, regional and national levels, 1990–2017: a population-based observational study. BMJ open. 2020;10(8):e036663.
73. Younossi ZM, Koenig AB, Abdelatif D, Fazel Y, Henry L, Wymer M. Global epidemiology of nonalcoholic fatty liver disease—Meta-analytic assessment of prevalence, incidence, and outcomes. Hepatology. 2016;64(1):73-84.
74. Croci I, Coombes JS, Sandbakk SB, Keating SE, Nauman J, Macdonald GA, et al. Non-alcoholic fatty liver disease: Prevalence and all-cause mortality according to sedentary behaviour and cardiorespiratory fitness. The HUNT Study. Progress in cardiovascular diseases. 2019;62(2):127-34.
75. Neuschwander-Tetri BA. Non-alcoholic fatty liver disease. BMC Med. 2017;15(1):45.
76. Holmer M, Melum E, Isoniemi H, Ericzon BG, Castedal M, Nordin A, et al. Nonalcoholic fatty liver disease is an increasing indication for liver transplantation in the Nordic countries. Liver Int. 2018;38(11):2082-90.
77. Charlton MR, Burns JM, Pedersen RA, Watt KD, Heimbach JK, Dierkhising RA. Frequency and Outcomes of Liver Transplantation for Nonalcoholic Steatohepatitis in the United States. Gastroenterology. 2011;141(4):1249-53.
78. Wong RJ, Aguilar M, Cheung R, Perumpail RB, Harrison SA, Younossi ZM, et al. Nonalcoholic Steatohepatitis Is the Second Leading Etiology of Liver Disease Among Adults Awaiting Liver Transplantation in the United States. Gastroenterology. 2015;148(3):547-55.
79. Beaton MD. Current treatment options for nonalcoholic fatty liver disease and nonalcoholic steatohepatitis. Can J Gastroenterol. 2012;26(6):353-7.
80. Lian C-Y, Zhai Z-Z, Li Z-F, Wang L. High fat diet-triggered non-alcoholic fatty liver disease: A review of proposed mechanisms. Chem Biol Interact. 2020;330:109199.
81. Sumida Y, Sumida Y, Yoneda M, Yoneda M. Current and future pharmacological therapies for NAFLD/NASH. J Gastroenterol. 2018;53(3):362-76.

82. Friedman SL, Neuschwander-Tetri BA, Rinella M, Sanyal AJ. Mechanisms of NAFLD development and therapeutic strategies. Nat Med. 2018;24(7):908-22.
83. Schattenberg JM, Galle PR. Animal Models of Non-Alcoholic Steatohepatitis: Of Mice and Man. Dig Dis. 2010;28(1):247-54.
84. Dowman JK, Tomlinson JW, Newsome PN. Pathogenesis of non-alcoholic fatty liver disease. QJM. 2010;103(2):71-83.
85. Watt MJ, Miotto PM, De Nardo W, Montgomery MK. The liver as an endocrine organ - linking NAFLD and insulin resistance. Endocr Rev. 2019;40(5):1367-93.
86. Donnelly KL, Smith CI, Schwarzenberg SJ, Jessurun J, Boldt MD, Parks EJ. Sources of fatty acids stored in liver and secreted via lipoproteins in patients with nonalcoholic fatty liver disease. J Clin Invest. 2005;115(5):1343-51.
87. Pierantonelli I, Svegliati-Baroni G. Nonalcoholic Fatty Liver Disease: Basic Pathogenetic Mechanisms in the Progression From NAFLD to NASH. Transplantation. 2019;103(1):e1-e13.
88. McPherson S, Hardy T, Henderson E, Burt AD, Day CP, Anstee QM. Evidence of NAFLD progression from steatosis to fibrosing-steatohepatitis using paired biopsies: Implications for prognosis and clinical management. J Hepatol. 2014;62(5):1148-55.
89. Machado MV, Diehl AM. Pathogenesis of Nonalcoholic Steatohepatitis. Gastroenterology. 2016;150(8):1769-77.
90. Cha J-Y, Kim D-H, Chun K-H. The role of hepatic macrophages in nonalcoholic fatty liver disease and nonalcoholic steatohepatitis. Lab Anim Res. 2018;34(4):133-9.
91. Koyama Y, Brenner DA. Liver inflammation and fibrosis. J Clin Invest. 2017;127(1):55-64.
92. Dewidar B, Meyer C, Dooley S, Meindl B, Nadja. TGF-β in Hepatic Stellate Cell Activation and Liver Fibrogenesis-Updated 2019. Cells. 2019;8(11):1419.
93. Anstee QM, Goldin RD. Mouse models in non-alcoholic fatty liver disease and steatohepatitis research. Int J Exp Pathol. 2006;87(1):1-16.
94. Machado MV, Michelotti GA, Xie G, Almeida Pereira T, de Almeida TP, Boursier J, et al. Mouse models of diet-induced nonalcoholic steatohepatitis reproduce the heterogeneity of the human disease. PLoS One. 2015;10(5):e0127991.
95. Li Z, Vance DE. Phosphatidylcholine and choline homeostasis. J Lipid Res. 2008;49(6):1187-94.
96. Cole LK, Vance JE, Vance DE. Phosphatidylcholine biosynthesis and lipoprotein metabolism. Biochimica et biophysica acta Molecular and cell biology of lipids. 2012;1821(5):754-61.
97. Vance DE. Role of phosphatidylcholine biosynthesis in the regulation of lipoprotein homeostasis. Curr Opin Lipidol. 2008;19(3):229-34.
98. Lau JKC, Zhang X, Yu J. Animal models of non-alcoholic fatty liver disease: current perspectives and recent advances. J Pathol. 2017;241(1):36-44.
99. Carr RM, Ahima RS. Pathophysiology of lipid droplet proteins in liver diseases. Exp Cell Res. 2016;340(2):187-92.
100. Motomura W, Inoue M, Ohtake T, Takahashi N, Nagamine M, Tanno S, et al. Up-regulation of ADRP in fatty liver in human and liver steatosis in mice fed with high fat diet. Biochem Biophys Res Commun. 2006;340(4):1111-8.
101. Straub BK, Stoeffel P, Heid H, Zimbelmann R, Schirmacher P. Differential pattern of lipid droplet-associated proteins and de novo perilipin expression in hepatocyte steatogenesis. Hepatology. 2008;47(6):1936-46.
102. Wang C, Zhao Y, Gao X, Li L, Yuan Y, Liu F, et al. Perilipin 5 improves hepatic lipotoxicity by inhibiting lipolysis. Hepatology. 2015;61(3):870-82.

103. Carr RM, Patel RT, Rao V, Dhir R, Graham MJ, Crooke RM, et al. Reduction of TIP47 improves hepatic steatosis and glucose homeostasis in mice. Am J Physiol Regul Integr Comp Physiol. 2012;302(8):R996-R1003.
104. Najt CP, Senthivinayagam S, Aljazi MB, Fader KA, Olenic SD, Brock JRL, et al. Liver-specific loss of Perilipin 2 alleviates diet-induced hepatic steatosis, inflammation, and fibrosis. Am J Physiol Gastrointest Liver Physiol. 2016;310(9):G726-G38.
105. Asimakopoulou A, Engel KM, Gassler N, Bracht T, Sitek B, Buhl EM, et al. Deletion of Perilipin 5 Protects Against Hepatic Injury in Nonalcoholic Fatty Liver Disease via Missing Inflammasome Activation. Cells. 2020;9(6):1346.
106. Desjardins P, Conklin D. NanoDrop Microvolume Quantitation of Nucleic Acids. J Vis Exp. 2010(45)2565.
107. Livak KJ, Schmittgen TD. Analysis of relative gene expression data using real-time quantitative PCR and the 2(T)(-Delta Delta C) method. Methods. 2001;25(4):402-8.
108. Michal Ganz Timea Csak Gyongyi S. High fat diet feeding results in gender specific steatohepatitis and inflammasome activation. World Journal of Gastroenterology. 2014;20(26):8525-34.
109. Matsushita N, Hassanein MT, Martinez-Clemente M, Lazaro R, French SW, Xie W, et al. Gender difference in NASH susceptibility: Roles of hepatocyte Ikkβ and Sult1e1. PLoS One. 2017;12(8):e0181052.
110. Rizki G, Arnaboldi L, Gabrielli B, Yan J, Lee GS, Ng RK, et al. Mice fed a lipogenic methionine-choline-deficient diet develop hypermetabolism coincident with hepatic suppression of SCD-1. J Lipid Res. 2006;47(10):2280-90.
111. Itagaki H, Shimizu K, Morikawa S, Ogawa K, Ezaki T. Morphological and functional characterization of non-alcoholic fatty liver disease induced by a methionine-choline-deficient diet in C57BL/6 mice. Int J Clin Exp Pathol. 2013;6(12):2683-96.
112. Jha P, Knopf A, Koefeler H, Mueller M, Lackner C, Hoefler G, et al. Role of adipose tissue in methionine–choline-deficient model of non-alcoholic steatohepatitis (NASH). Biochimica et biophysica acta Molecular basis of disease. 2014;1842(7):959-70.
113. Gao G, Chen F-J, Zhou L, Su L, Xu D, Xu L, et al. Control of lipid droplet fusion and growth by CIDE family proteins. Biochimica et biophysica acta Molecular and cell biology of lipids. 2017;1862(10):1197-204.
114. Vogel C, Marcotte EM. Insights into the regulation of protein abundance from proteomic and transcriptomic analyses. Nat Rev Genet. 2012;13(4):227-32.
115. Perlman RL. Mouse models of human disease: An evolutionary perspective. Evol Med Public Health. 2016;2016(1):170-6.
116. Ibrahim SH, Hirsova P, Malhi H. Animal Models of Nonalcoholic Steatohepatitis: Eat, Delete, and Inflame. Dig Dis Sci. 2016;61(5):1325-36.
117. Rinella ME, Green RM. The methionine-choline deficient dietary model of steatohepatitis does not exhibit insulin resistance. J Hepatol. 2004;40(1):47-51.
118. Ishimoto T, Lanaspa MA, Rivard CJ, Roncal-Jimenez CA, Orlicky DJ, Cicerchi C, et al. High-fat and high-sucrose (western) diet induces steatohepatitis that is dependent on fructokinase. Hepatology. 2013;58(5):1632-43.
119. Asgharpour A, Cazanave SC, Pacana T, Seneshaw M, Vincent R, Banini BA, et al. A diet-induced animal model of non-alcoholic fatty liver disease and hepatocellular cancer. J Hepatol. 2016;65(3):579-88.
120. Eccleston HB, Andringa KK, Betancourt AM, King AL, Mantena SK, Swain TM, et al. Chronic Exposure to a High-Fat Diet Induces Hepatic Steatosis, Impairs Nitric Oxide Bioavailability, and Modifies the Mitochondrial Proteome in Mice. Antioxid Redox Signal. 2011;15(2):447-59.

121. Velázquez KT, Enos RT, Bader JE, Sougiannis AT, Carson MS, Chatzistamou I, et al. Prolonged high-fat-diet feeding promotes non-alcoholic fatty liver disease and alters gut microbiota in mice. World journal of hepatology. 2019;11(8):619-37.
122. Garibyan L, Avashia N. Research Techniques Made Simple: Polymerase Chain Reaction (PCR). Journal of investigative dermatology. 2013;133(3):e6.
123. Kozera B, Rapacz M. Reference genes in real-time PCR. Journal of applied genetics. 2013;54(4):391-406.
124. Eisenberg E, Levanon EY. Human housekeeping genes, revisited. Trends Genet. 2013;29(10):569-74.
125. Kirkwood BR, Sterne JAC. Comparison of means from several groups: analysis of variance. Essential medical statistics, Second edition. Malden, USA: Blackwell; 2003. p. 80-86.
126. Ghasemi A, Zahediasl S. Normality tests for statistical analysis: a guide for non-statisticians. Int J Endocrinol Metab. 2012;10(2):486-9.
127. Rinella ME, Elias MS, Smolak RR, Fu T, Borensztajn J, Green RM. Mechanisms of hepatic steatosis in mice fed a lipogenic methionine choline-deficient diet. J Lipid Res. 2008;49(5):1068-76.
128. Benny Hung-Junn C, Lan L, Antoni P, Susumu T, Vijayalakshmi N, William CH, et al. Protection against Fatty Liver but Normal Adipogenesis in Mice Lacking Adipose Differentiation-Related Protein. Mol Cell Biol. 2006;26(3):1063-76.
129. Giménez-Andrés M, Emeršič T, Antoine-Bally S, D'Ambrosio JM, Antonny B, Derganc J, et al. Exceptional stability of a perilipin on lipid droplets depends on its polar residues, suggesting multimeric assembly. Elife. 2021;10.
130. Yang P, Wang Y, Tang W, Sun W, Ma Y, Lin S, et al. Western diet induces severe nonalcoholic steatohepatitis, ductular reaction, and hepatic fibrosis in liver CGI-58 knockout mice. Sci Rep. 2020;10(1):4701-.
131. Kvam IS. Characterisation of Plin4 null mice - Absence of Plin4 results in lower hepatic expression of genes involved in lipogenesis [masteroppgave]. Oslo, Norway: University of Oslo; 2019. p. 26 and 29.
132. Zhang E, Cui W, Lopresti M, Mashek MT, Najt CP, Hu H, et al. Hepatic PLIN5 signals via SIRT1 to promote autophagy and prevent inflammation during fasting. J Lipid Res. 2020;61(3):338-50.
133. Francque S, Verrijken A, Caron S, Prawitt J, Paumelle R, Derudas B, et al. PPARα gene expression correlates with severity and histological treatment response in patients with non-alcoholic steatohepatitis. J Hepatol. 2015;63(1):164-73.
134. Abdelmegeed MA, Yoo S-H, Henderson LE, Gonzalez FJ, Woodcroft KJ, Song B-J. PPARalpha expression protects male mice from high fat-induced nonalcoholic fatty liver. J Nutr. 2011;141(4):603-10.
135. Régnier M, Polizzi A, Smati S, Lukowicz C, Fougerat A, Lippi Y, et al. Hepatocyte-specific deletion of Pparα promotes NAFLD in the context of obesity. Sci Rep. 2020;10(1):6489.
136. Chakravarthy MV, Lodhi IJ, Yin L, Malapaka RRV, Xu HE, Turk J, et al. Identification of a Physiologically Relevant Endogenous Ligand for PPARα in Liver. Cell (Cambridge). 2009;138(3):476-88.
137. Kirsch R, Clarkson V, Shephard EG, Marais DA, Jaffer MA, Woodburne VE, et al. Rodent nutritional model of non-alcoholic steatohepatitis: Species, strain and sex difference studies. J Gastroenterol Hepatol. 2003;18(11):1272-82.
138. Lee Y-H, Kim SH, Kim S-N, Kwon H-J, Kim J-D, Oh JY, et al. Sex-specific metabolic interactions between liver and adipose tissue in MCD diet-induced non-alcoholic fatty liver disease. Oncotarget. 2016;7(30):46959-71.

139. Williams CD, Stengel J, Asike MI, Torres DM, Shaw J, Contreras M, et al. Prevalence of Nonalcoholic Fatty Liver Disease and Nonalcoholic Steatohepatitis Among a Largely Middle-Aged Population Utilizing Ultrasound and Liver Biopsy: A Prospective Study. Gastroenterology. 2011;140(1):124-31.
140. Ballestri S, Nascimbeni F, Baldelli E, Marrazzo A, Romagnoli D, Lonardo A. NAFLD as a Sexual Dimorphic Disease: Role of Gender and Reproductive Status in the Development and Progression of Nonalcoholic Fatty Liver Disease and Inherent Cardiovascular Risk. Adv Ther. 2017;34(6):1291-326.
141. Chen KL, Madak-Erdogan Z. Estrogens and female liver health. Steroids. 2018;133:38-43.
142. Yoshihiro K, Shinichi K, Yuichi Y, Norihiro C, Takashi K, Mina H, et al. Estrogen deficiency worsens steatohepatitis in mice fed high-fat and high-cholesterol diet. Am J Physiol Gastrointest Liver Physiol. 2011;301(6):1031-43.

6 Appendix

Appendix 1. Recipe for high salt solution

Appendix 2. Primers used in RT-qPCR

Appendix 3. Solutions used for Western blotting

Appendix 4. Antibodies used for Western blotting

Appendix 5. Western blot of Plin4

Appendix 1. Recipe for high salt solution

Recipe for high salt solution. Abbreviations: NaCl: Sodium Chloride; Na: Sodium; RNase: Ribonuclease; H_2O: water

Components	**Final concentrations**	**10 ml**	**Stock solutions**
NaCl	1.5 M	3 ml	5 M NaCl
Na-Acetate (pH 5.5)	0.8 M	2,67 ml	3 M Na-Acetate
RNase free H_2O	-	4,33 ml	

Appendix 2. Specific primer pairs used for RT-qPCR

Gene name	Accession number	Forward primer	Reverse primer
Plin1	NM_001113471.1	ACCTGGAGGAAAAGATCCCG	TTCGAAGGCGGGTAGAGATG
Plin2	NM_007408.3	GGGCTAGACAGGATGGAGGA	CACATCCTTCGCCCCAGTTA
Plin3	NM_025836.3	CGAAGCTCAAGCTGCTATGG	TCACCATCCCATACGTGGAAC
Plin4	NM_020568.3	ACCAACTCACAGATGGCAGG	AGGCATCTTCACTGCTGGTC
Plin5	NM_001077348.1	GGTGAAGACACCACCCTAGC	CCACCACTCGATTCACCACA
Cidea	NM_007702.2	CCTTAAGGGACAACACGCAT	TTGCTTGCAGACTGGGACATA
Cideb	NM_009894.3	GTCTGTGATCATAAGCGGACAGT	GTGTTAGCACTCCACGTAGCA
Cidec	NM_001301295.1	GCTCACAGCTTGGAGGACC	CCATCTTCCTCCAGCACCAG
Pnpla2	NM_001163689.1	CACTCACATCTACGGAGCCT	TAATGTTGGCACCTGCTTCAC
G0s2	NM_008059.3	TCTCTTCCCACTGCACCCTA	GGATCAGCTCCTGCACACTT
Abhd5	NM_026179.2	TCCCTTTAACCCCTTGGCTG	GCCTCAAACGCTGCACTAGA
Lipe	NM_001039507.2	TCACGCTACACAAAGGCTGC	GAGAGTCTGCAGGAACGGC
Lyz	NM_013590.4	AATCGTTGTGAGTTGGCCAGAA	TCGGTCTCCACGGTTGTAGT
Adgre	XM_006523601.1	TGTACGTGCAACTCAGGACT	TCCTGGAGCACTCATCCACA
Marco	NM_010766.3	ACTCCAGAGGGAGAGCACTT	TCTCTGTGCCCCGACAATTC
Il1b	XM_006498795.3	GCTGAAAGCTCTCCACCTCA	TGTCGTTGCTTGGTTCTCCT
Il6	NM_031168.2	TGATGGATGCTACCAAACTGGA	GGTACTCCAGAAGACCAGAGG
Tnf	NM_013693.3	CCACCACGCTCTTCTGTCTAC	CTGATGAGAGGGAGGCCATT
Dmpk	NM_001190491.2	AACTACAGGAGGCCGAGGTC	AGATGGGAAGGTGGATCCGTG
Tgfb1	NM_011577.2	ATGCCAACTTCTGTCTGGGA	GTTGGTTGTAGAGGGCAAGGA
Col1a1	NM_007742.4	CTGACGCATGGCCAAGAAGAC	CCTCGGGTTTCCACGTCTCA
Srebf1a	NM_001313979.1	GGCCGAGATGTGCGAACTG	GTTGTTGATGAGCTGGAGCATGT
Srebf1c	XM_006532716.2	GGAGCCATGGATTGCACATTT	CAGCATAGGGGGCGTCAAA
Chrebpα	NM_021455.4	CCTCTTCGAGTGCTTGAGCC	GGATCTTGTCCCGGCATAGC
Chrebpβ	XM_006504483.2	GACCCGAGGTCCCAGGAT	CACTTGGGAGAGACCAGCTT
Acaca	NM_133360.2	TACGCTGACCGAGAAAGCAG	GATCTACCCGACGCATGGTT
Fasn	NM_007988.3	CTTCGGCTGCTGTTGGAAGTC	GTGTTCGTTCCTCGGAGTGAG
Ppara	NM_001113418.1	ACTACGGAGTTCACGCATGT	GTCGTACACCAGCTTCAGCC
Ppard	NM_011145.3	ACATGGAATGTCGGGTGTGC	CGAGCTTCATGCGGATTGTC
Pparg	NM_001127330.1	TTGCTGTGGGGATGTCTCAC	AACAGCTTCTCCTTCTCGGC
Cpt1a	NM_013495.2	CCCAGCTGTCAAAGATACCGT	GCTGTCATGCGTTGGAAGTC
Acox1	NM_015729.3	AATCTGGAGATCACGGGCACTT	GTCTTGGGGTCATATGTGGCAG

Appendix 3. Solutions used for Western blotting

RIPA buffer

5 ml 1 M Tris-HCl

3 ml 5 M NaCl

4 ml 25% NP-40

5 ml 10% Sodium deoxycholate

0.5 ml 20% SDS

4 ml 0.5 M EDTE

78.5 ml MQ H_2O

4x Laemmli buffer

1.5 ml 1 M Tris-HCl pH 6.5

3 ml of 1 M DTT (dithiothreitol)

0.6 g of SDS (sodium dodecyl sulfate)

30 mg of Bromophenol blue

2.4 ml of Glycerol

MQ H_2O was added until the final volume reached 7.5 mL

10x Running buffer

30.3 g 250 mM Tris-base

144 g 1.92 M Glycine

10 g SDS (sodium dodecyl sulfate)

MQ H_2O was added until the solution reached 1 L

1x Running buffer

100mL 10x running buffer

900mL MQ H_2O

10x TBS-T

24.2 g 200 mM Tris-base

80.15 g 1370 mM NaCl

1 M HCl

MQ H_2O was added until the solution reached 1 L

1x TBS-T

100 mL 10x TBS-T

1 mL Tween-20

MQ H_2O was added until the solution reached 1 L

Blocking buffer

5g BSA (bovine serum albumin)

100 mL 1x TBS-T

Appendix 4. Antibodies used for Western blotting.

Primary-and secondary- antibodies used for Western Blotting

Target protein	**Dilution**	**Product name and number**	**Secondary antibody**
Plin2 (C-terminus)	1:1000 in 2.5% BSA in TBS-T	Progen, Cat# GP43	Guinea Pig
Plin3 (N-terminus)	1:2000 in 2.5% BSA in TBS-T	Progen, Cat#GP36	Guinea pig
Plin5 (C-terminus)	1:1000 in 2.5% BSA in TBST	Progen, Cat#GP31	Guinea pig
α-SMA	1:1000 in 2.5% BSA in TBST	Cell Signalling Technology, 19245s	Rabbit
GAPDH	1:1000 in 2.5% BSA in TBST	Santa Cruz Biotechnology, sc-25778	Rabbit

Appendix 5. Western blot of Plin4

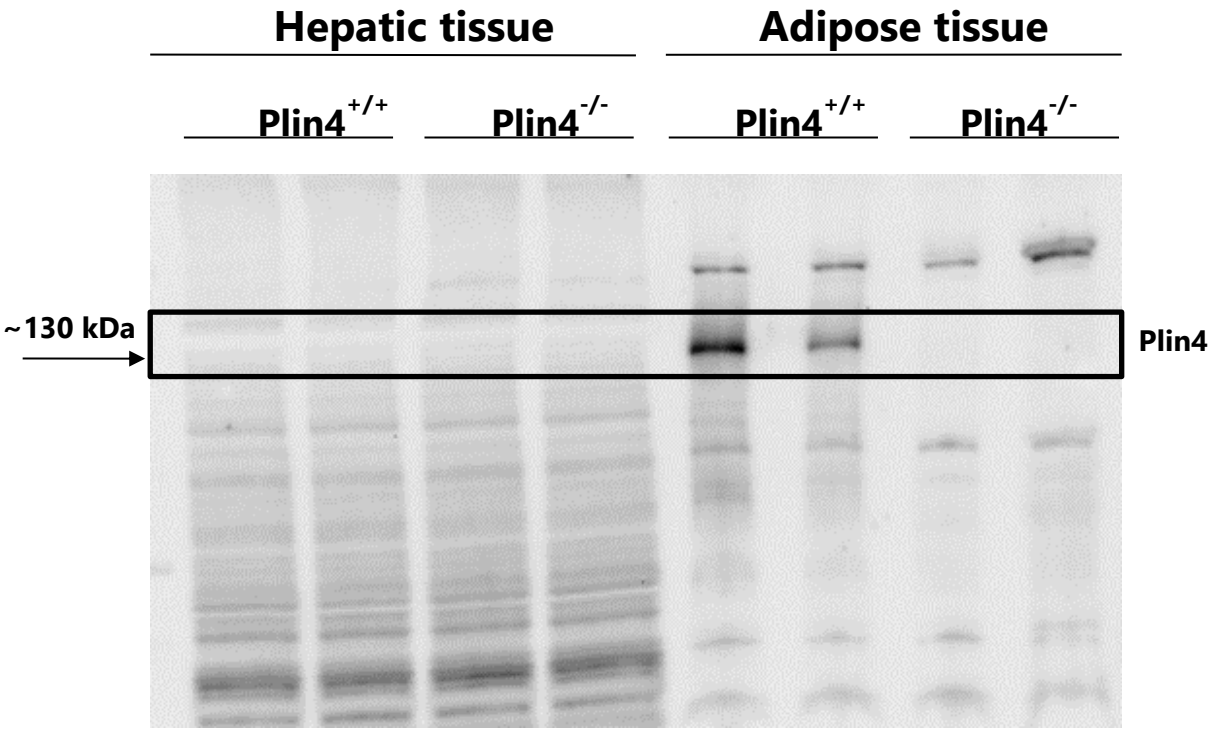

Western blot of Plin4 in hepatic and adipose tissue from *Plin4*$^{+/+}$ and *Plin4*$^{-/-}$ mice. Liver lysate samples from *Plin4*$^{+/+}$ and *Plin4*$^{-/-}$ male mice fed a methionine and choline deficient diet for two weeks. Adipose tissue lysate samples from *Plin4*$^{+/+}$ and *Plin4*$^{-/-}$ female mice fed a high-fat diet for ~10 weeks. 30 µg protein was loaded per lane. Homemade N-terminus Plin4 antibody (diluted 1:750 in 2.5% TBST-T) was used to detect Plin4.